Sediment Dispersal Patterns of the Outer Shelf to Upper Slope Paleocene-Eocene Wilcox Group, South-Central Texas Coast

Hongliu Zeng[1], William A. Ambrose[1], and Wenlong Xu[2]

[1]Bureau of Economic Geology, Jackson School of Geosciences, University of Texas at Austin,
University Station, Box X, Austin, Texas 78713–8924, U.S.A.

[2]Excellong, Inc., 77 Sugar Creek Center Blvd., Ste. 215, Sugar Land, Texas 77478, U.S.A.

ABSTRACT

Applying wavelet-phase adjustment and attribute analysis to interpret lithology and stratal slices to deduce seismic geomorphology, we interpreted a 960 mi^2 (2500 km^2) 3D seismic volume, wireline log, and sparse-core data along the south-central Texas coast to investigate the sediment dispersal patterns in transition from on-shelf to the deepwater. The sequence-stratigraphic architecture of the Wilcox Group revealed four subbasins separated by major growth faults, which roughly correlated to a lower Wilcox subunit, a middle Wilcox subunit, and two upper Wilcox subunits. Each of the subbasins developed over an average 3.5 m.y. period. We prepared lithology-calibrated stratal slice maps to reveal high-resolution (33–130-ft [10–40 m]) sediment-dispersal patterns and associated systems tracts in subbasin C of the upper Wilcox. Recognized depositional systems include: (1) incised valley fills (IVFs) and relict on-shelf deltas on an exposed shelf; (2) off-shelf lowstand prograding deltaic systems composed of lobate deltaic sandstone bodies; and (3) off-shelf slope fans best characterized by point-source, fanlike channel/levee systems. At least four episodes of shallow LST (lowstand system tract) incised valleys containing 33–130 ft (10–40 m) of gross sandstone inferred from wireline logs were identified. These thin, sandstone-rich IVFs on exposed shelf are coeval with thick, sand–shale mixed slope fans and LST deltaic systems along growth faults, suggesting that large amounts of sediment may have bypassed these channels and may have been trapped between the fault zones in multiple subbasins. In addition to deep-cut submarine canyons (e.g., Yoakum Canyon), these IVFs provided an alternative fairway that may have transported sandy LST deposits and associated reservoirs seaward of the Cretaceous shelf edge to the deepwater Gulf of Mexico.

INTRODUCTION

Mobile shale and growth fault-controlled sedimentation is typical in many basins in the world (e.g., Gulf of Mexico, Niger Delta, and Bohai Bay Basin in China). Especially in the Tertiary Gulf Coast of Texas, depositional systems formed in such a setting have been important hydrocarbon reservoirs. Bebout et al. (1982) documented such stratigraphic architecture and depositional style in the Tertiary Gulf Coast of Texas. Fed by large rivers draining the continental interior, thick clastic sediments were associated with an unstable shelf margin and syndepositional faulting. Growth faults were initiated where major rivers deposited significant volumes of sands onto unconsolidated offshore shales (Bebout et al., 1982). The Wilcox fault zone—which separates on-shelf and deepwater depositional systems—is

the oldest of a series of major growth-fault trends bordering the northern Gulf of Mexico and extending south to the Frio, Miocene, and younger formations of offshore Gulf of Mexico (Fig. 1). Deltaic systems have long been recognized in on-shelf areas (Fisher and McGowen., 1967; Edwards, 1981). In the deepwater Gulf of Mexico region, thick, basin-floor fan sediments have been identified in recent years (Galloway, 2000, 2011; Zarra, 2007; Fulthorpe et al., 2014). The transition zone between the two geographic regions in south-central Texas, however, has undergone limited study. Galloway (2000) reported on the deep Yoakum and Hardin canyons in the Central Texas and far East Texas coastal plain that were activated and filled during Wilcox time. Zeng et al. (2014) suggested a transition from shallow incised valleys to prograding deltaic wedges and slope fans during third-order lowstand, similar to the transition in better-known Frio subbasins (Brown et al., 2004, 2005).

Investigations by Brown et al. (2004, 2005) revealed widespread, sea-level, shale tectonics and growth fault–controlled subbasins in the Oligocene Frio Formation in the Corpus Christi region (Fig. 1), which were formed during third-order (1–1.3 m.y.) cycles. To explain how those subbasins were developed,
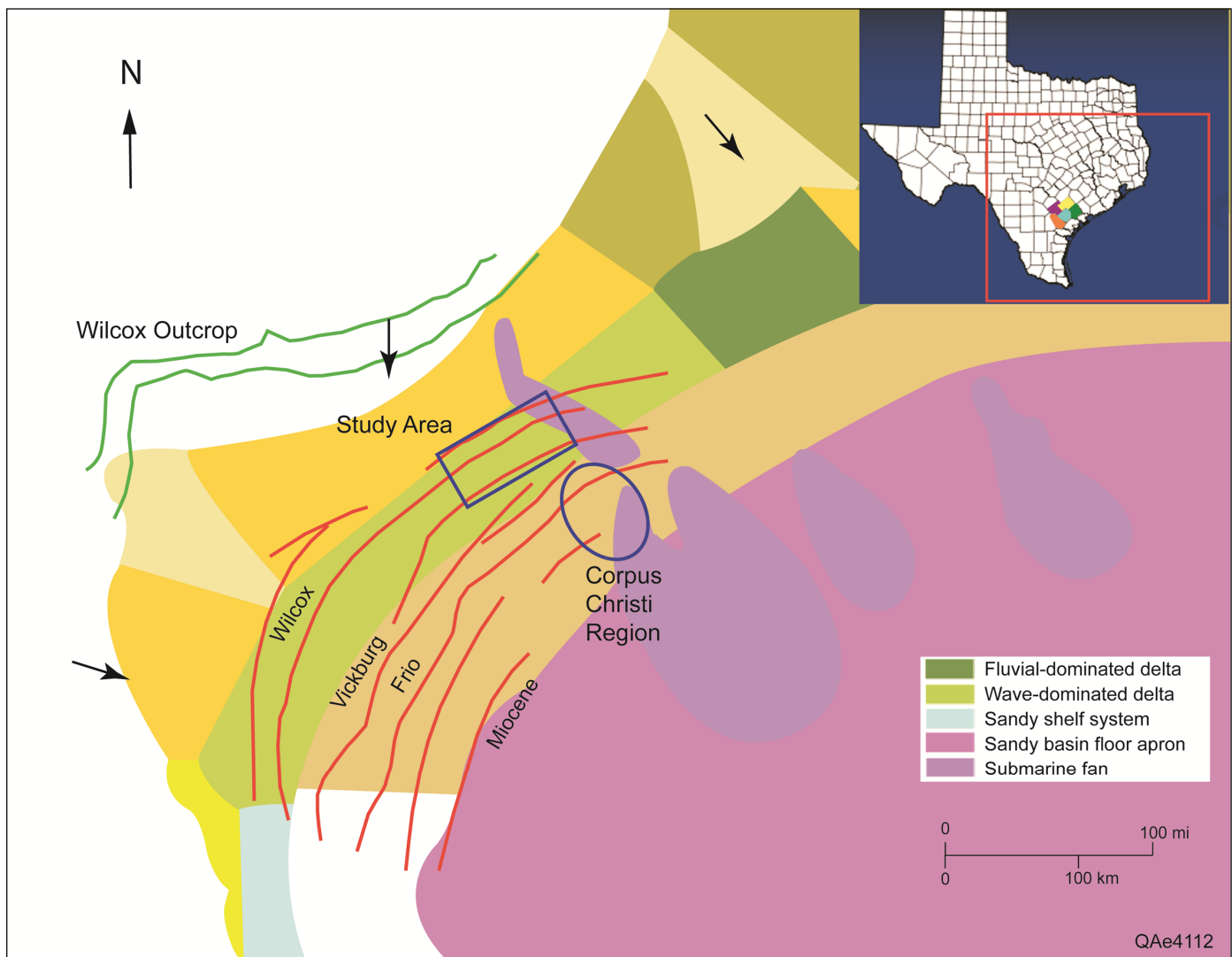
Figure 1. General tectonic and depositional setting in study area. Paleogeographic map for upper (UW) Wilcox unit I from Fulthorpe et al. (2014). Distribution of major growth-fault zones in the south-central Texas Gulf Coast is modified from Montgomery (1997).

Brown et al. (2004) proposed models that focused on dynamic depositional processes that occurred during relative lowstands of sea level. Intraslope subbasins were formed as a result of interaction among sediment supply, growth faulting, and relative sea-level change. Each third-order lowstand systems tract essentially filled one intraslope subbasin. The weight of sediment supplied by entrenched rivers overloaded lowstand slopes, initiated gravity faulting, mobilized mud, and produced shale ridges. An accommodation, therefore, formed between the updip growth fault and the downdip shale ridge. The seismic representation of this syndepositional process is a series of diachronous reflection wedges separated by major growth faults. Treviño et al. (2003) and Hammes et al. (2004) published detailed case studies from the Mustang Island and Redfish Bay areas, respectively. Zeng et al. (2007) further investigated unique seismic expressions of higher-order sequences and systems tracts, especially slope fans and lowstand prograding wedges, in Corpus Christi Bay sub-basins (Fig. 1).

One of the poorly documented aspects of Frio-type sub-basins is the seismic mapping of shallowly incised valley fills (IVFs) on the exposed shelf to the landward, upthrown, footwall side of the subbasin, which otherwise would provide evidence of the existence of ancient entrenched rivers. In previous studies

(e.g., Zeng et al., 2007), seismic reflections that are correlated to the third-order lowstand systems tracts in this zone are almost, if not completely, missing, probably because the sediments on the exposed shelf were severely eroded (Brown et al., 2004, 2005). As a result, existence and distribution of IVFs were largely implied. Encouraged by the fact that IVFs have been documented in the Miocene Oakville Formation in the nearby Redfish Bay area of South Texas (Loucks et al., 2011), we believe that a large 3D seismic survey in the Bee/Goliad region (Fig. 1), which includes comparable reflections of the Wilcox on-shelf sedimentary record and was available to this study, might shed more light on the visualization of the complete picture of systems tracts and facies-dispersal patterns in similar depositional settings.

A seismic sedimentology based study demonstrates the extraordinary development of IVFs in a large Wilcox exposed shelf, and of prograding wedges and slope fans in multiple Wilcox subbasins. Although data quality and availability does not allow definitive correlations, by tentatively matching on-shelf IVFs to off-shelf lowstand systems tract (LST) prograding wedges and slope fans, links are visualized between all three elements, which is helpful in understanding the history and reservoir potential of Wilcox depositional systems in space and time.

DATA AND METHODOLOGY

General chronology of Cenozoic stratigraphy of Gulf of Mexico (Fig. 2A, from Galloway et al., 2011) includes multiple episodes of deposition (depisodes of Galloway [2000] terminology). The Wilcox Group is inferred to have formed during a period of 14 m.y. (Galloway, 2011, in Figure 2A). Comparing Wilcox and Frio in a regional profile (Fig. 2B) shows that these two depisodes have a similar general stratigraphic and structural style, both of which experienced significant sediment supply and continental margin growth. The later Paleocene–early Eocene Wilcox Group records the first major impulse of sediment supply of the Tertiary, which can be divided into lower, middle, and upper units (Galloway, 2011), followed by another significant continental outbuilding during deposition of the Oligocene Frio Formation after several smaller depositional episodes (Queen City through Vicksburg, Fig. 2B). Thickness, outbuilding distance, and sediment volume are comparable between these two depisodes. Therefore, knowledge gained in the study of Frio should provide guidance in the investigation of the relatively less known Wilcox Group. A similar seismic-sedimentology-based approach (Zeng et al., 2007) is applied to this study.

The study area encompasses a 5 county region (largely in Bee and Goliad counties) that is covered by a large 3D seismic volume of approximately 960 mi^2 (2500 km^2) (Fig. 3). Roughly paralleling the Texas coastline, the stacked and migrated data volume is characterized by a bin size of 110 ft (33.5 m) at a sample rate of 4 ms. Although this area has been densely drilled, only limited deep wells and few cores are available for this study (Fig. 3). Most of the wells have spontaneous potential and/or gamma ray and resistivity log curves. Velocity data are available from sonic logs from several wells. Biostratigraphic data are rare in the study area.

Well-to-seismic correlation was established using synthetic seismograms (e.g., Juan Alvarado et al. well, Fig. 4). The major character tie between synthetics and well-site seismic traces appears clear. Major seismic stratigraphic reference horizons are relatively strong amplitude events (peaks and troughs) in the synthetic trace and are traceable throughout the 3D survey (e.g., SB1–SB6), which were then used to define third-order sequences in the study area using the approach of Van Wagoner et al. (1990). The higher-order sequence-stratigraphic framework then can be established using techniques discussed in Van Wagoner et al. (1990) and Mitchum et al. (1993). They described upward-coarsening parasequences as the basic building blocks of stratigraphy, which can be applied to the Wilcox study.

A major challenge in interpreting sequence stratigraphy and depositional systems in high resolution is that the 3D seismic
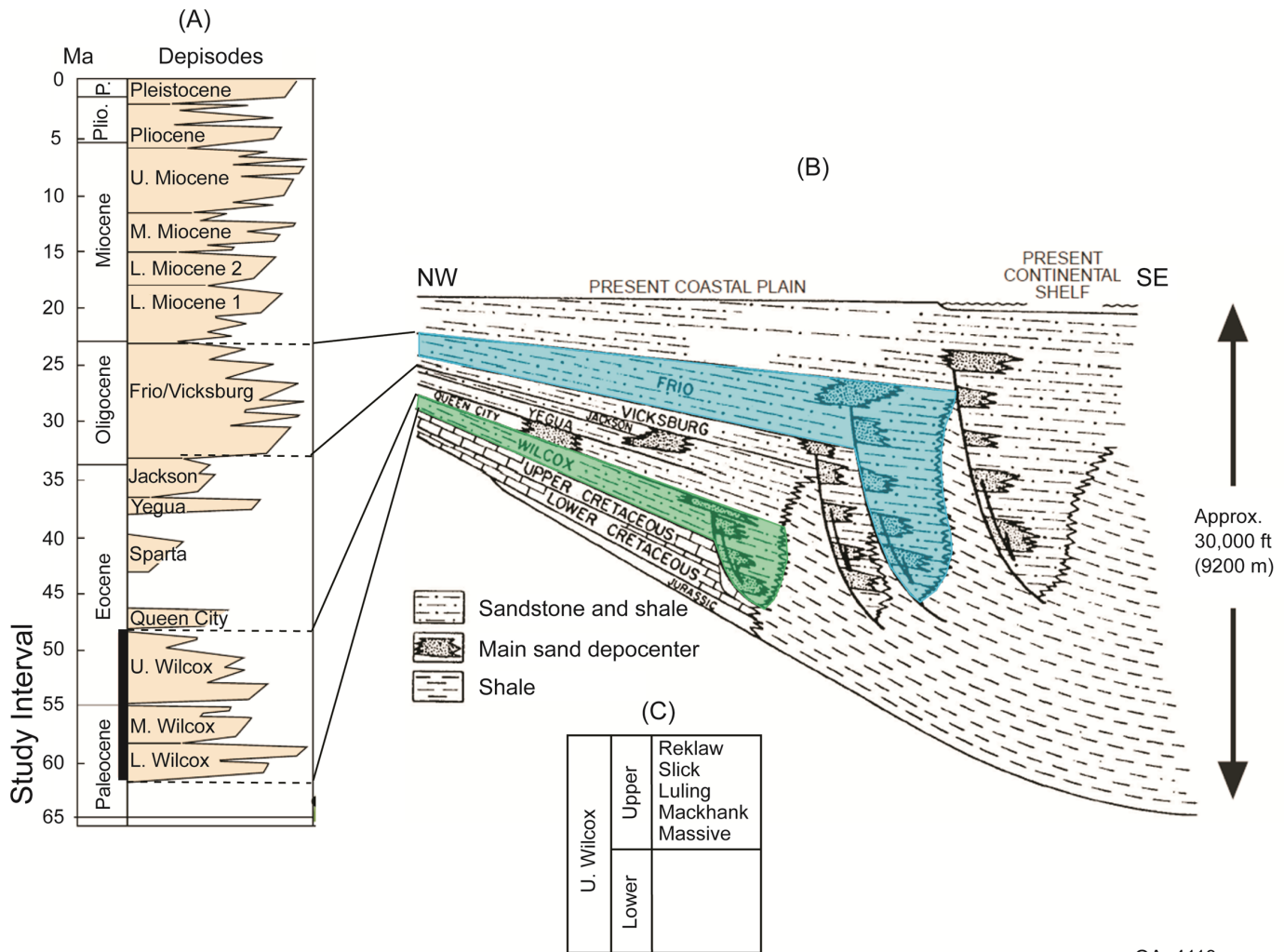

Figure 2. General stratigraphy and shale tectonic style in southern Texas Gulf of Mexico. (A) Chronology of Cenozoic stratigraphy of Gulf of Mexico (from Galloway et al., 2011, courtesy of the Geological Society of America) (B) General Tertiary stratigraphic architecture in the southern Texas Gulf Coast (modified after Bebout et al., 1982). (C) Subdivision of the upper Wilcox unit (from Hargis, 2009, courtesy of the South Texas Geological Society).
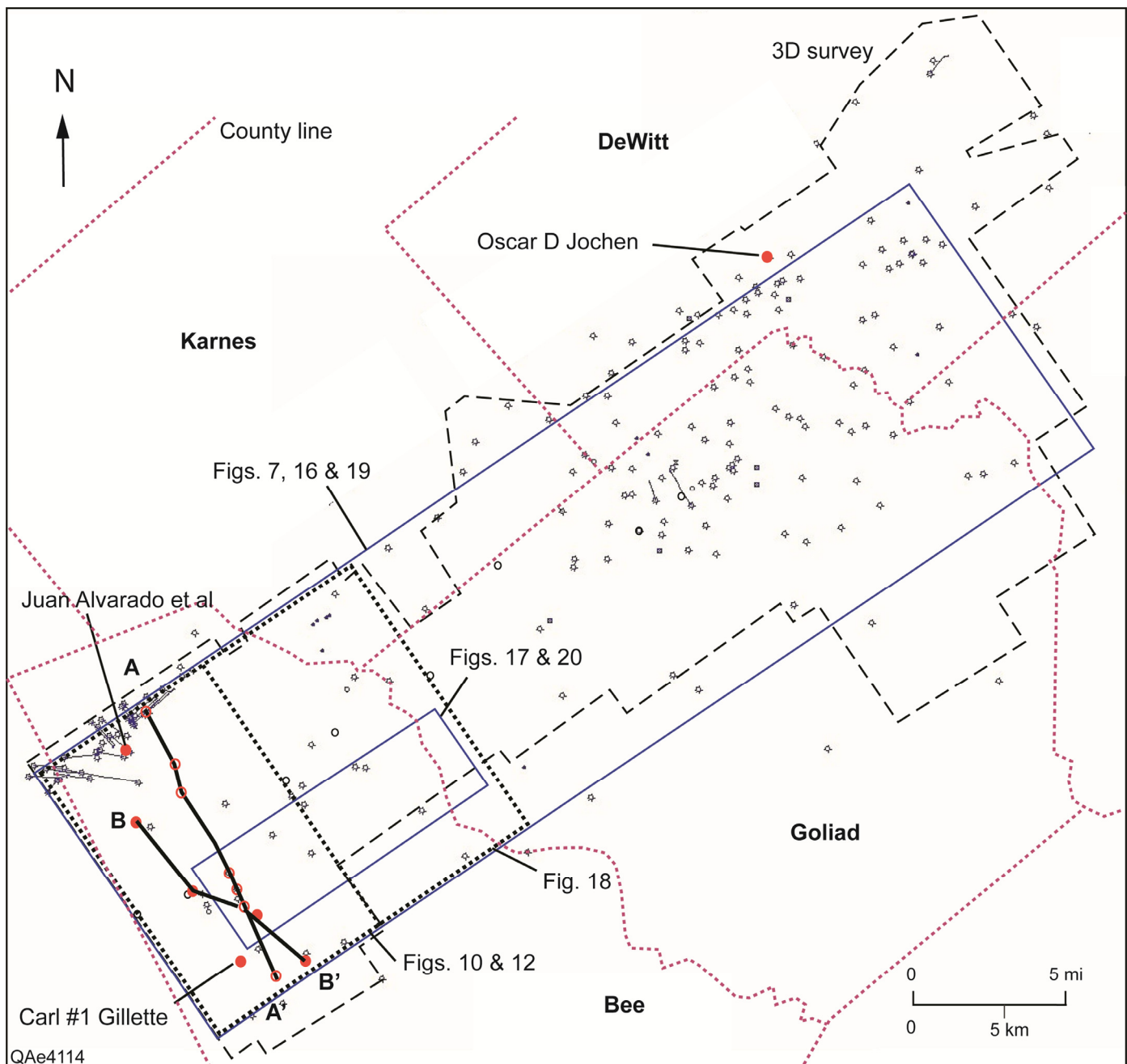
Figure 3. 3D seismic survey and well locations in the Bee and Goliad region. See Figure 1 for location.

data are low in vertical resolution. With a dominant frequency of around 25 Hz at the Wilcox interval, the calculated vertical resolution (a quarter wavelength) is about 20 ms, or 130 ft (40 m) (at 13,000 ft/s, or roughly 4000 m/s). The detectable limit is related to data quality and is estimated about 1/25 wavelength, or 3 ms (6 m) based on Sheriff's (2002) definition. Because most of the sandstone units in incised valleys, deltas, and slope fans in the study interval are near or thinner than the resolution limit, identifying and correlating high-frequency sequences using conventional seismic analysis would be a formidable, if not an impossible, task. A seismic-sedimentologic approach, which aims at mapping depositional systems at detectable limit (Zeng and Hentz, 2004), is therefore necessary.

As illustrated in Figure 5, the first step of the workflow was structural interpretation. Faults were identified by reflection offsets and time-structure maps were made to highlight roll-over anticlines separated by major faults in subbasins. Then, a high-resolution sequence framework was established first by third-order sequence analysis of seismic data and high-order wireline log correlation. An adjustment was performed of the wavelet phase to -90° to convert seismic volume to relative impedance volume for thin-bed lithology. The integral of zero-phase trace is not recommended because of lower resolution. Proper seismic attributes were selected for imaging sandstone body geometry and depositional elements. Stratal slices were prepared between geologic time-equivalent, reference seismic events for different subbasins and systems tracts. The final step in the workflow was seismic-sedimentologic mapping of various depositional systems for sediment-dispersal patterns at a higher-order sequence level by integrating seismic geomorphologic analysis on stratal slices with core and wireline log analysis in wells.
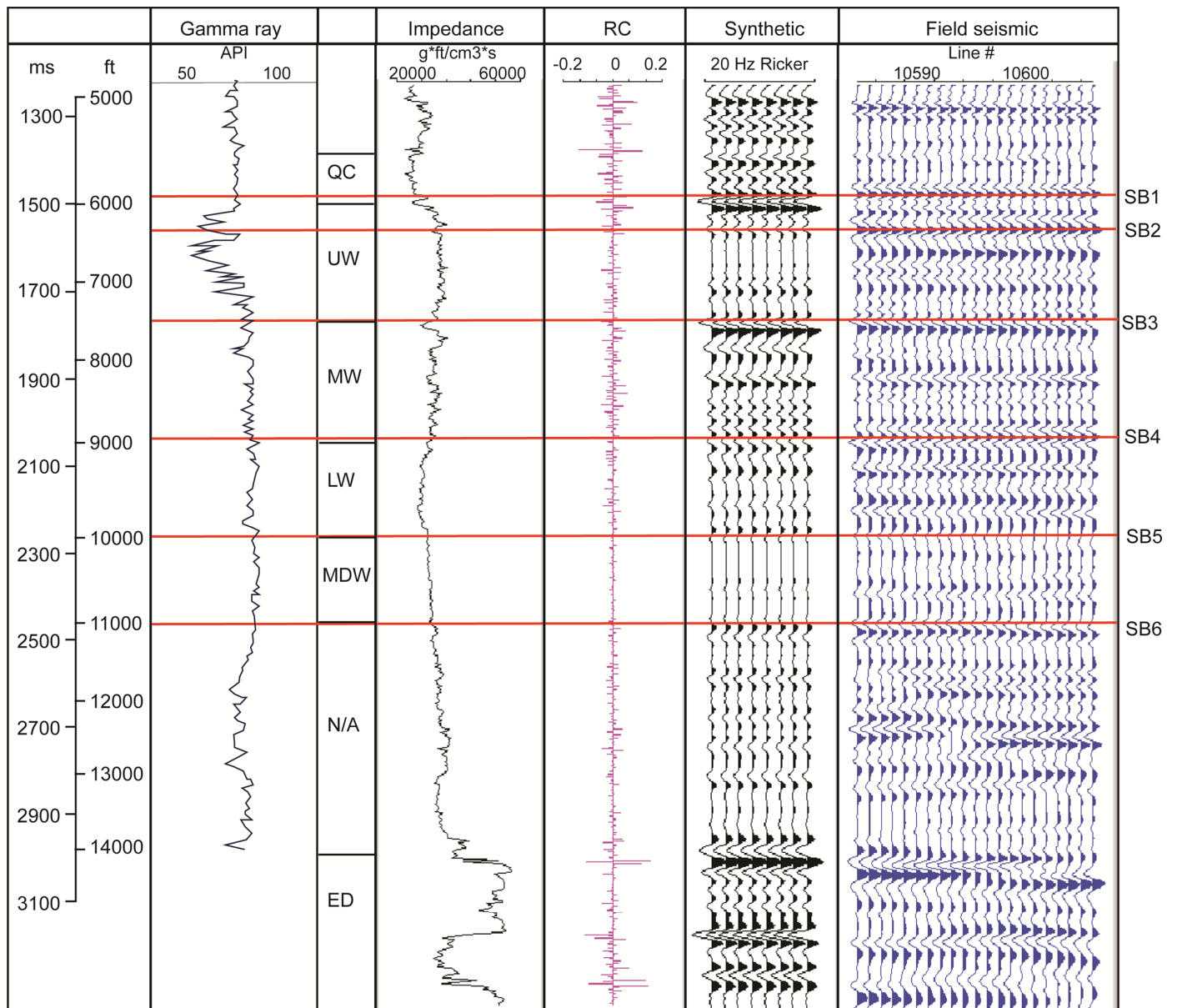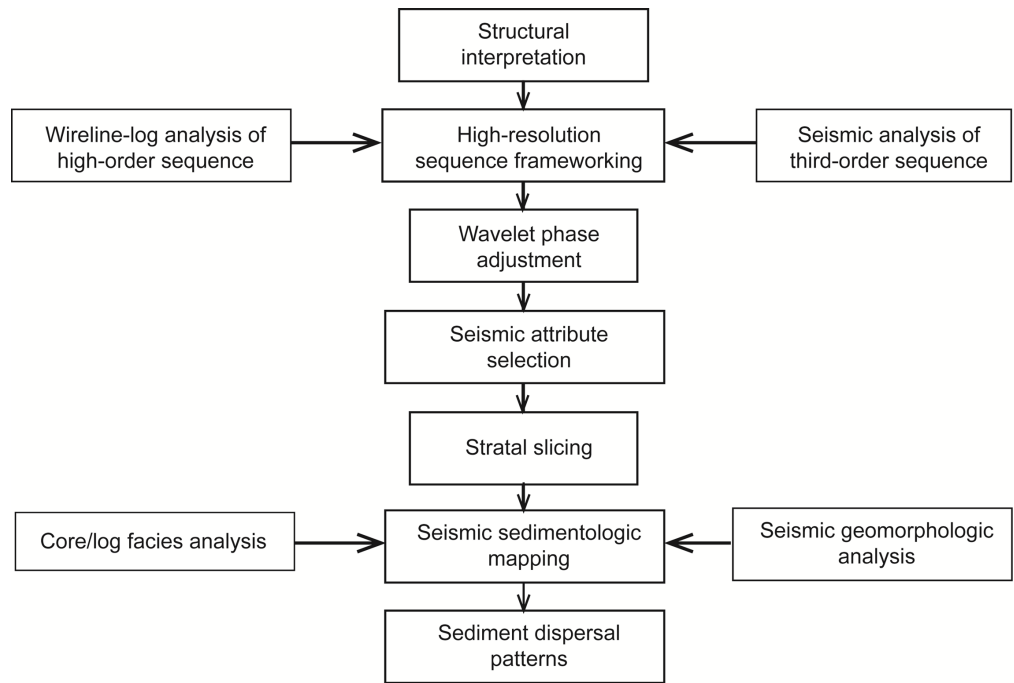
CM = Cool Mountain
QC = Queen City
UW = upper Wilcox
MW = middle Wilcox

LW = lower Wilcox
MDW = Midway
N/A = Navarro + Austin
ED = Edwards

QAe4115

Figure 4. Synthetic seismogram of Juan Alvarado et al well. The well-site seismic traces are zero-phased, with a dominant frequency of 20 Hz (deeper section) to 30 Hz (shallower section). The synthetic trace was created with sonic log and a 20 Hz Ricker wavelet. Synthetic events correlate well to stratigraphic boundaries (and major reflection events SB1 through SB6).

Integration of 3D seismic, core, and wireline log data is a valid method of defining stratigraphic architecture and associated systems tracts that has been successfully applied to many basins. Seismic geomorphology (Posamentier, 2000, 2001) provides a popular platform for such integration. The plan-view geometry (pattern) of seismic amplitude is interpreted based on modern analogs of depositional systems. With dense well control (core and wireline logs), many seismic geomorphologic patterns can be interpreted in terms of lithofacies and reservoir quality (e.g., Carter, 2003). Yet in many cases, such as in this study, availability of wireline logs and core data is limited, preventing a robust seismic-geomorphologic interpretation of raw seismic images in a large area. A calibration, or preconditioning, of seismic data such that lithology and/or other key reservoir parameters (e.g., porosity) can be easily linked to seismic attribute patterns is highly desirable, especially for high-resolution (reservoir) studies. In seismic sedimentology, an analysis of seismic-lithology preconditioned data is based on the core- and wireline log–derived relationship between lithology and acoustic impedance, which are then used to generate stratal slices for the study of seismic geomorphology (e.g., Zeng and Hentz, 2004; Zeng et al., 2007; Aconcha et al., 2008; Loucks et al., 2011; Cheng et al., 2015).

Figure 5. Workflow to interpret major structural features and high-resolution depositional units.

```
                              Structural
                            interpretation
                                  │
                                  ▼
Wireline-log analysis of    High-resolution         Seismic analysis of
  high-order sequence   →  sequence frameworking ←   third-order sequence
                                  │
                                  ▼
                            Wavelet phase
                             adjustment
                                  │
                                  ▼
                          Seismic attribute
                             selection
                                  │
                                  ▼
                            Strative slicing
                                  │
                                  ▼
   Core/log facies        Seismic sedimentologic    Seismic geomorphologic
     analysis         →        mapping          ←        analysis
                                  │
                                  ▼
                          Sediment dispersal
                             patterns
```

QAe4116

SHALE TECTONICS–CONTROLLED STRUCTURAL FRAMEWORK AND THIRD-ORDER SEQUENCE STRATIGRAPHY

Structural and third-order sequence-stratigraphic relationships around the Wilcox subbasins can be characterized in dip-oriented, well-seismic section A–A' (Fig. 6). Four subbasins (A–D, Fig. 6) are bounded by major growth faults (black) that have significant throws (as large as 6000 ft [1929 m]). As individual depocenters of the fault-related expansions, each subbasin was interpreted to have a much thinner (1500 ft [457 m]), nonexpansional feeder section at the landward, footwall side of the boundary fault. By carefully correlating to synthetic seismograms (Fig. 4), subbasins A–D are inferred to have formed during depositions of lower and middle Wilcox units, and of subunits 1 and 2 of upper Wilcox, over a total period of 14 m.y. (Galloway, 2011, in Figure 2A). Specifically, subunits 1 and 2 of upper Wilcox (subbasins C and D, Fig. 6) represent two third-order sediment wedges accumulated on average in a 3.5 m.y. period, respectively. Defining the two third-order sequences in the subunits 1 and 2 of upper Wilcox are sequence boundaries SB1, SB2, and SB3 that can be traced throughout the 3D survey as prominent seismic reference events (Fig. 6). These sequence boundaries were interpreted as type 1 unconformities, with subtle seismic truncations throughout the 3D survey (Fig. 6). Third-order maximum flooding surfaces can only be correlated inside the subbasin (e.g., mfs in subbasin C, Fig. 6) near a downlapping surface that coincided with a high gamma ray, low resistivity kick in wireline logs (Oehlke well, Fig. 6).

At the proximal (northwest) side of each subbasin, strata are rolled over against the boundary growth fault. Formation thickness is maximal near the fault, gradually thinning toward the top of the rollover structure. Basinward, strata become flat or down dipping, until terminated by the next major boundary fault. Some rollover anticlines are complicated by smaller compensation faults (red in Figure 6). Beneath the traceable reflections are deep-seated, chaotic reflection bodies, which demonstrate shale-ridge characteristics similar to those reported in the Frio Formation (e.g., Treviño et al., 2003; Brown et al., 2004; Hammes et

al., 2004). One or more interpreted shale ridges lie directly beneath the anticline, extending between the boundary faults (Fig. 6).

A time-structure map (Fig. 7A) further characterizes dis-tribution of the faults and rollover structures and their relationship to shale ridges in various subbasins throughout the 3D survey. Three northeastern-trending major faults (dashed lines) separate four subbasins. Subbasins A through D become successively deeper basinward (Fig. 7B). Complicated by smaller compensational faults, the rollover anticlines (+ sign) in each subbasin (especially B and C) are alternated by synclines (- sign). Shale ridges were observed beneath each of the anticlines, similar to those seen in seismic section A–A' (Fig. 6). Shale ridges occur beneath each of the anticlines. The synclines coincide with depocenters along each subbasin that were related to accommodation created by flowing of soft shale to adjacent anticlines.

HIGH-FREQUENCY SEQUENCE STRATIGRAPHY AND DEPOSITIONAL SYSTEMS

Wireline Log Correlation

Stratigraphic surfaces correlated from wireline logs in this study include flooding surfaces and an unconformity. Flooding surfaces are inferred from both core and wireline log data. Flooding surfaces interpreted from core data are composed of silty, dark-gray mudstone. These flooding surfaces, when inferred from wireline log responses, occur within continuous, low-resistivity zones that vertically bound upward-coarsening successions. An unconformity occurs at the base of sandstone beds with blocky and upward-fining wireline log responses. These sandstones beds are locally >80 ft (>24.4 m) thick and are inferred to locally truncate underlying strata.

A third-order sequence, bounded by unconformities at sequence boundaries, includes multiple depositional episodes at the scale of individual fourth-order parasequences defined by Van Wagoner et al. (1990). Locally, thin (commonly 50 to 150 ft
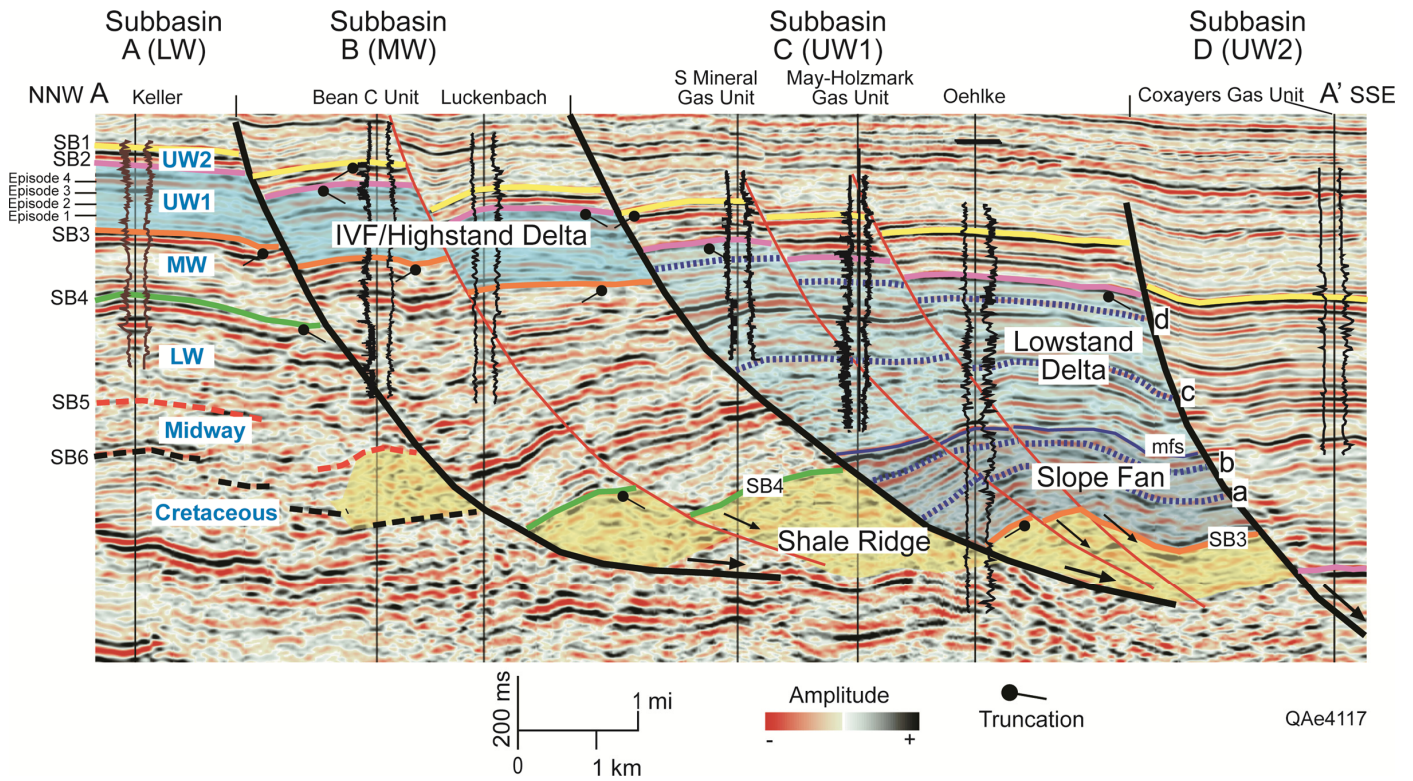
Figure 6. Dip-oriented, well-seismic section A–A' showing structural and stratigraphic architecture of the Wilcox subbasins. The seismic data are -90° phased. Wireline logs shown include spontaneous potential (SP) and/or gamma ray (GR) (left) and resistivity (right). See Figure 3 for location.
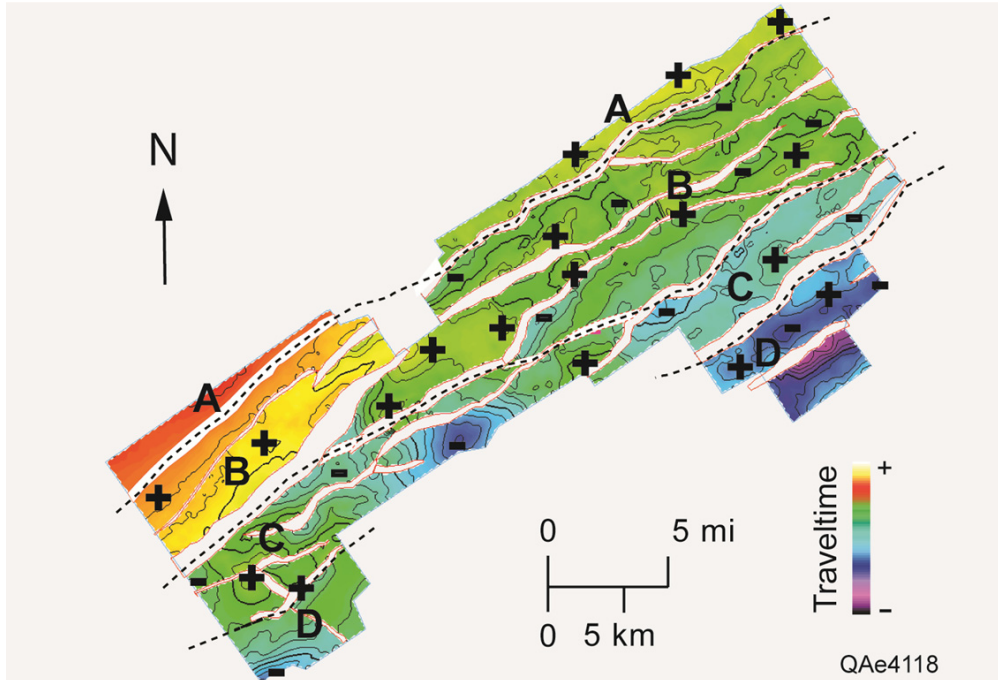

Figure 7. Time-structure map showing distribution of faults and rollover structures (anticlines with "+" sign and synclines with "-" sign) in subbasins A through D. See Figure 3 for position.

[15.2 to 45.7 m]) depositional episodes in the upper Wilcox Group and, most bounded by high-frequency flooding surfaces, are correlated and mapped. By resolving the upper Wilcox stratigraphic succession into numerous, high-frequency depositional episodes or parasequences defined by Van Wagoner et al. (1990), it is possible to more accurately portray the sandstone-body geometry at reservoir scales and to more accurately depict the

paleogeography of deltaic, coastal-plain, shoreface, and shelf depositional systems.

Wireline-log correlation of section A–A' (Fig. 8) revealed sequence-stratigraphic and facies architecture at third- and higher-order sequences around subbasin C. The overall upward-coarsening nature of spontaneous potential and/or gamma ray logs in subbasin C (e.g., Oehlke well in Figure 8) implies an
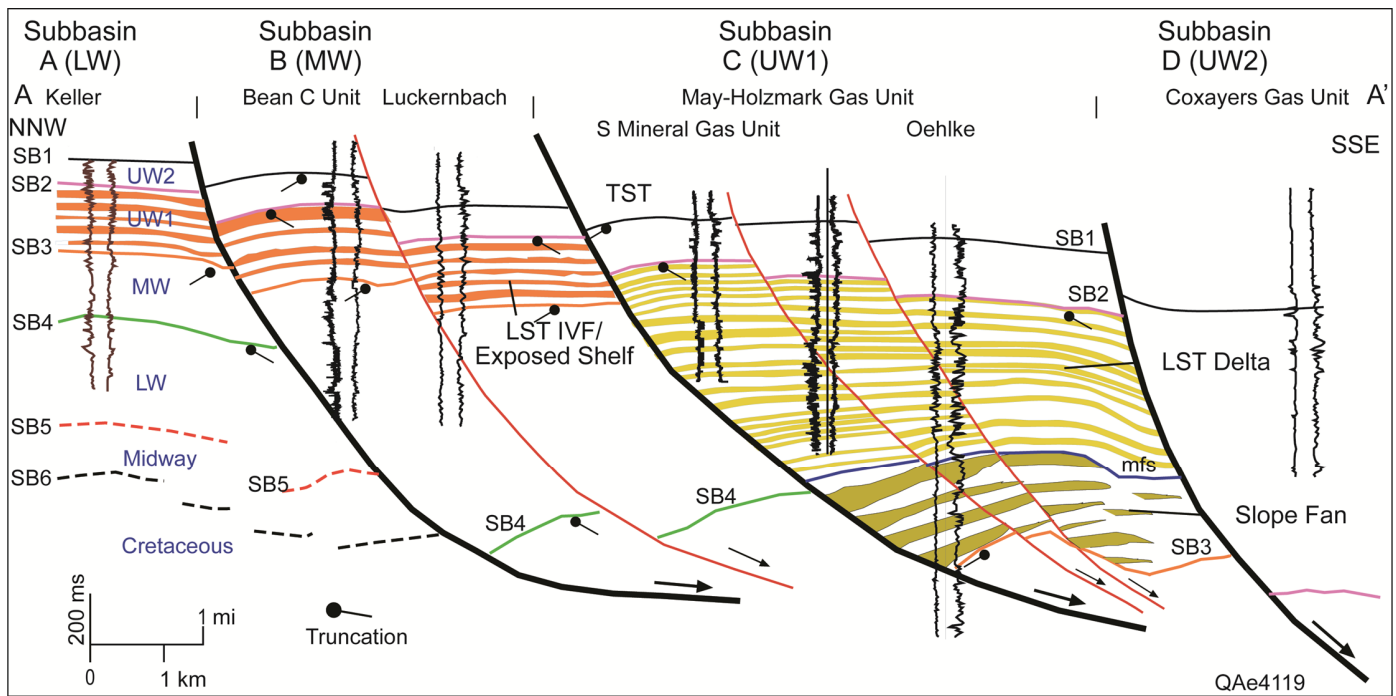
Figure 8. Dip-oriented well section A–A' revealing higher-order sequence-stratigraphic and facies architecture at third- and higher-order sequences around subbasin C. Major stratigraphic/seismic boundaries are copied from Figure 6.

overall progradational history. Major third-order depositional systems are characterized by distinctive wireline log lithofacies motifs similar to those in Frio subbasins (Zeng et al., 2007), which can be correlated to distinctive seismic facies characteristics. The sediments in the third-order lowstand slope-fan system are multi-cycle (fourth or higher-order sequences) interbedded shale, shaly sandstone, and siltstone (Oehlke well, Fig. 8). The sandstones are tight in the Oehlke well and show an upward-fining pattern in other wells. These sediments are inferred to be turbidite deposits of slope fans. Seismically, this system comprises the most discontinuous reflection packages, directly overlying the deep shale ridges (Fig. 6). The disconformably overlying, third-order, lowstand prograding deltaic complex on the surface of mfs is composed of multi-cycle interbedded sandstone and shale deposited in LST deltaic systems. The continuity of deltaic lithofacies is greater than for those in the slope fan, evidenced by greater seismic continuity (Fig. 6). Superposed on top of the prograding complex is a sandy LST related to subbasin D (subunit 2 of upper Wilcox), followed by a shaly third-order transgressive systems tract (TST) containing continuous condensed sections that can be correlated throughout the seismic survey area. Correlation of higher-order (fourth- and fifth-order) sequences within individual third-order systems tracts can be made only symbolically using wireline logs without accurately identifying tops and bottoms between wells because of the limit of well density and lack of seismic resolution.

By comparison, third-order, on-shelf LSTs (IVFs and exposed shelf) on the landward, footwall fault block against the subbasin display less characteristic wireline log pattern (Fig. 8) and seismic facies (Fig. 6). Multiple upward-fining or blocky sandstone beds at higher-order sequence level are visible in some wells but missing in others, which were inferred to be fluvial-channel deposits or LST prograding-wedge (PW) distributary-channel deposits. Shaly, upward-coarsening patterns indicate relict on-shelf deltaic sediments. Subparallel, variable amplitude/continuity seismic reflections (Fig. 6) imply a more or less tabular formation with significant internal changes in lithofacies and sandstone thickness.

Core Description

No conventional cores in intervals are interpreted as third-order systems tracts of slope fans and IVFs. Fortunately, several conventional cores in the study area sampled the distal portion of the third-order LST delta systems in the upper Wilcox unit (Fig. 2B; Massive, Mackhank, Luling, Slick, and Reklaw units).

The Carl No. 1 Gillette core, spans most of a 100 ft (30.5 m), upward-coarsening section inferred from the wireline log response in Figure 9. The Carl No. 1 Gillette well is located on the northwestern margin of the strike-elongate trend of >80 ft (>24.4 m) of gross sandstone (Fig. 10). The overall spontaneous potential response for the cored interval in the Carl No. 1 Gillette well is upward-coarsening to serrate, from which interbedded sandstone and mudstone is inferred (Fig. 9). The Carl No. 1 Gillette core contains parts of two separate parasequences that record high-frequency, regressive-transgressive cycles. The top of the lower parasequence is inferred to be above an upward-fining section at 10,194 ft (3107.9 m). (Fig. 9). The base of an upper parasequence coincides with a silty mudstone bed at 10,194 ft (3107.9 m).   This upper parasequence, which is upward-coarsening to 10,180 ft (3103.7 m), extends to the top of the cored interval.

Facies Mapping

Gross sandstone is defined using a cutoff value of ~30% from a baseline of maximum gamma ray deflection indicating minimum clay content. This value is determined by calibrating wireline log response to values of gross sandstone measured in the core description of the Carl No. 1 Gillette well core, located in Figure 10. For wells without the gamma ray curve, the spontaneous potential and resistivity curves are used to determine gross sandstone values. Depositional systems and facies interpretations, as well as paleogeographic reconstructions for each upper Wilcox stratigraphic interval in the study area, are based on integration of wireline log character, gross-sandstone thickness maps, seismic attribute maps, and available core data. Sandstone

Figure 9. Log response and core description of the Carl No. 1 Gillette well, located in Figure 10.
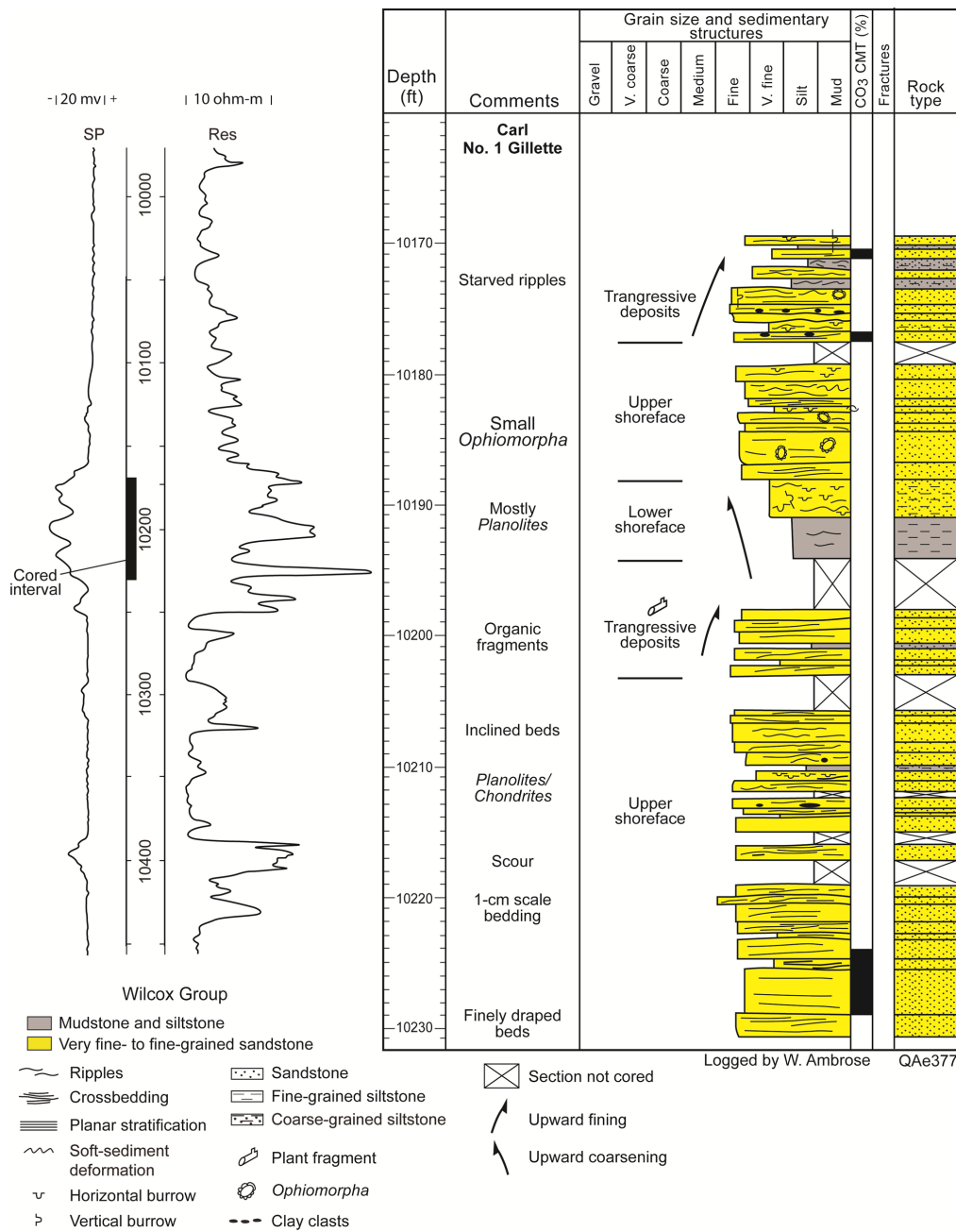
body geometry and distribution in gross-sandstone thickness maps of upper Wilcox intervals are compared to those observed in both modern and ancient depositional settings to interpret depositional systems, facies, and to reconstruct the paleogeography.

A gross-sandstone thickness map of the undivided Luling unit illustrates narrow (0.5–3.0 mi [0.8–4.8 km]), dip-elongate (south and southeast) trends with more than 80 ft (>24.4 m) of gross sandstone, mainly developed in the northern and northwestern part of the study area. These dip-elongate gross-sandstone trends intersect an extensive, southwest–northeast-oriented trend of more than 60 ft (>18 m) of gross sandstone in the southern part of the study area (Fig. 10). The strike-elongate trend of more than 80 ft (>24.4 m) of gross sandstone is up to 2 mi (3.2 km) wide, in contrast to the dip-elongate trend to the north, where belts of more than 80 ft (24.4 m) of gross sandstone are typically only 0.5 mi (0.8 km) wide.

The upper part of the Luling unit, characterized primarily by blocky log responses, truncates the lower Luling unit in the north and northwest part of the mapping area (Fig. 11). This sandy interval has an overall dip-elongate gross-sandstone geometry, with southwest-trending depositional axes defined by belts of more than 70 ft (>21.3 m) of gross sandstone that vary in width from less than 2000 ft (<610 m) to more than 10,000 ft (3050 m) (Fig. 12). These depositional axes have an anastomosing character, particularly in the northwestern part of the study area. This interval is sandstone poor in the southern and southeastern part of the study area, where it commonly contains less than 20 ft (<6 m) of gross sandstone. A boundary separates sandstone-rich and sandstone-poor areas of the map (Fig. 12).

The upper Luling unit represents high-order, lowstand, incised-valley deposits that truncate highstand lower-coastal-plain, backbarrier, and barrier-core deposits in the underlying lower Luling interval in the northern and northwestern parts of the mapping area. The predominantly blocky wireline log response in this interval, developed principally in the northern and northwestern part of the mapping area, represents amalgamated bed-load

Figure 10. Gross-sandstone thickness of the undivided Luling unit in northern Bee County. Map area shown in Figure 3. Stratigraphic cross section B–B' shown in Figure11.
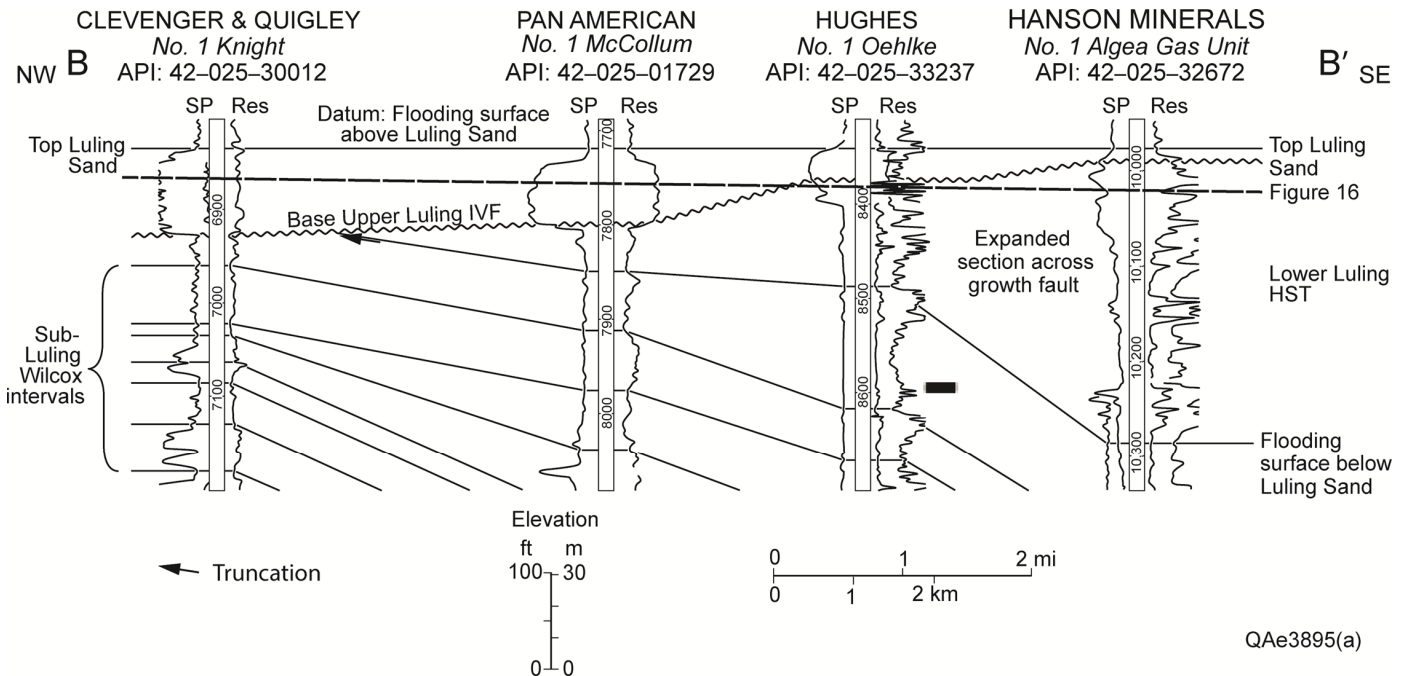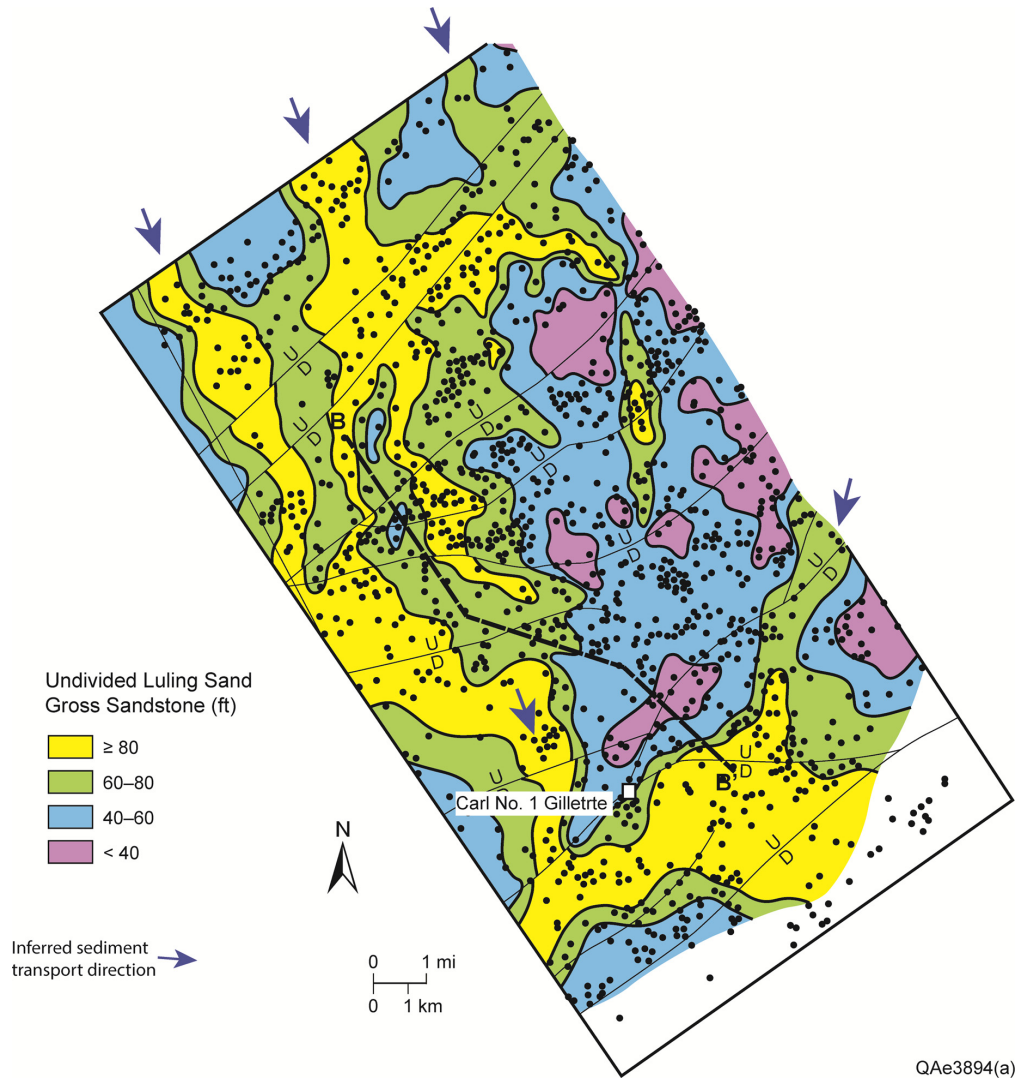

Undivided Luling Sand
Gross Sandstone (ft)

- ≥ 80
- 60–80
- 40–60
- < 40

Carl No. 1 Gilletrte

N

Inferred sediment transport direction

0   1 mi
0   1 km

QAe3894(a)

CLEVENGER & QUIGLEY
No. 1 Knight
API: 42–025–30012

PAN AMERICAN
No. 1 McCollum
API: 42–025–01729

HUGHES
No. 1 Oehlke
API: 42–025–33237

HANSON MINERALS
No. 1 Algea Gas Unit
API: 42–025–32672

NW B   B' SE

SP Res   Datum: Flooding surface   SP Res   SP Res   SP Res

Top Luling Sand   above Luling Sand   Top Luling Sand
                                                                                          Figure 16

Base Upper Luling IVF   Expanded   Lower Luling HST
                                                              section across
Sub-Luling   growth fault
Wilcox intervals
                                                                                       Flooding surface below Luling Sand

Elevation
ft   m
100 – 30

← Truncation

0   1   2 mi
0   1   2 km

0 – 0

QAe3895(a)

Figure 11. Stratigraphic cross-section B–B' depicting lowstand incised valley-fill deposits in the Upper Luling unit that truncate highstand wave-dominated shoreline deposits in the lower Luling unit. See Figure 10 for location.

Figure 12. Gross-sandstone thickness of the Upper Luling unit in northern Bee County. Map area shown in Figure 3. Stratigraphic cross section B–B' shown in Figure11.
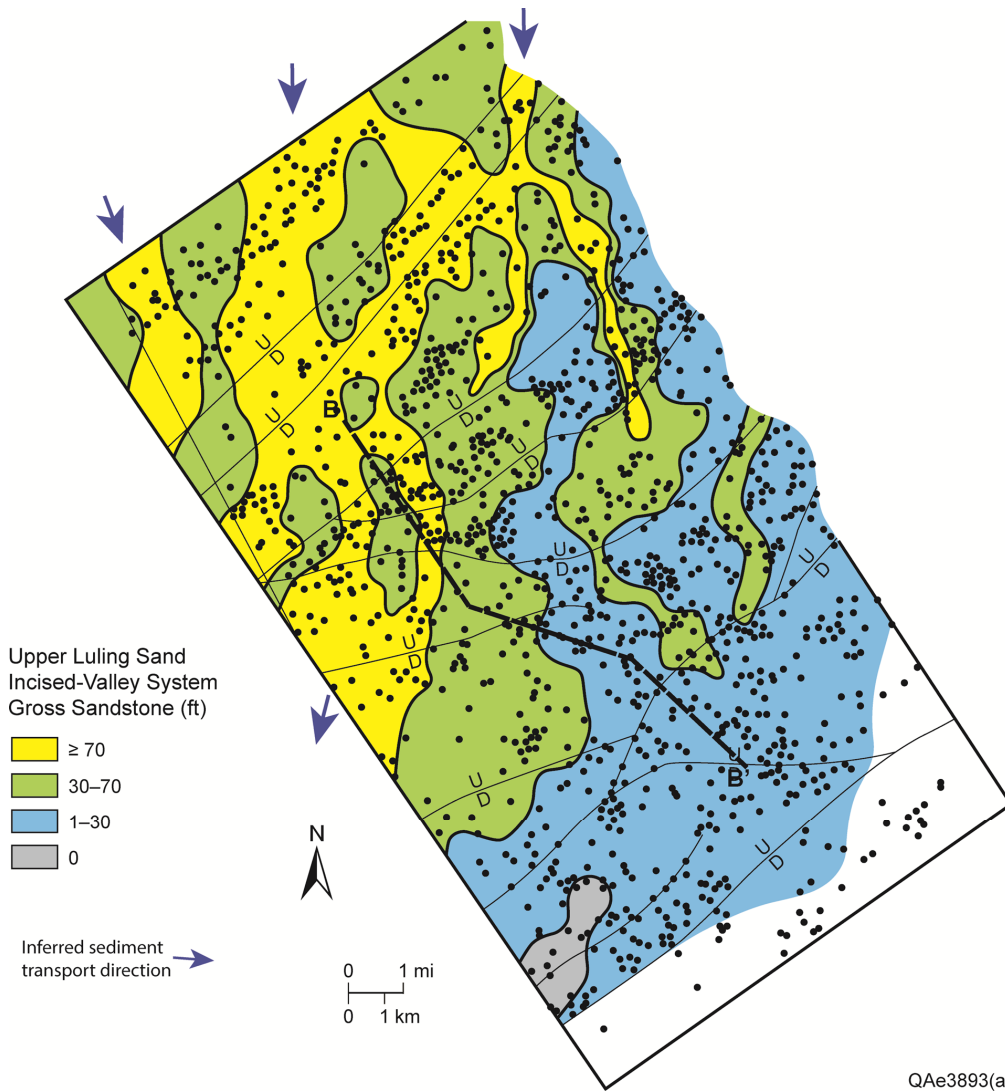
fluvial channel-fill deposits. Facies analogs in other ancient stratigraphic successions for fluvial deposits in the upper Luling interval include bed-load fluvial channel deposits in the East Texas Field (Ambrose et al., 2009).

Modern bed-load fluvial deposits are commonly composed of coarse-grained, sandy longitudinal and transverse bars that form by downstream migration in braided-river systems (Ore, 1963; Smith, 1970; Boothroyd, 1972; Smith, 1970; Lunt et al., 2004). Lateral continuity of these fluvial channel-fill sandstone beds is variable but commonly great in large composite channel fills (Galloway, 1977; Schumm, 1981). Vertical continuity in these systems can also be great where successive channel fills are amalgamated into multistory sandstone bodies like those in Woodbine valley fills in the East Texas Field (Ambrose et al., 2009).

On vertical seismic sections, these reservoir-level (33–130 ft [10–40 m]), higher-order (fourth- and fifth-order) packages within third-order tracts are difficult to track and map. However, as previous studies (e.g., Zeng et al., 2007) have shown, such thin sequences can be studied with stratal slices by using a seismic-sedimentologic approach, as described in the following sections.
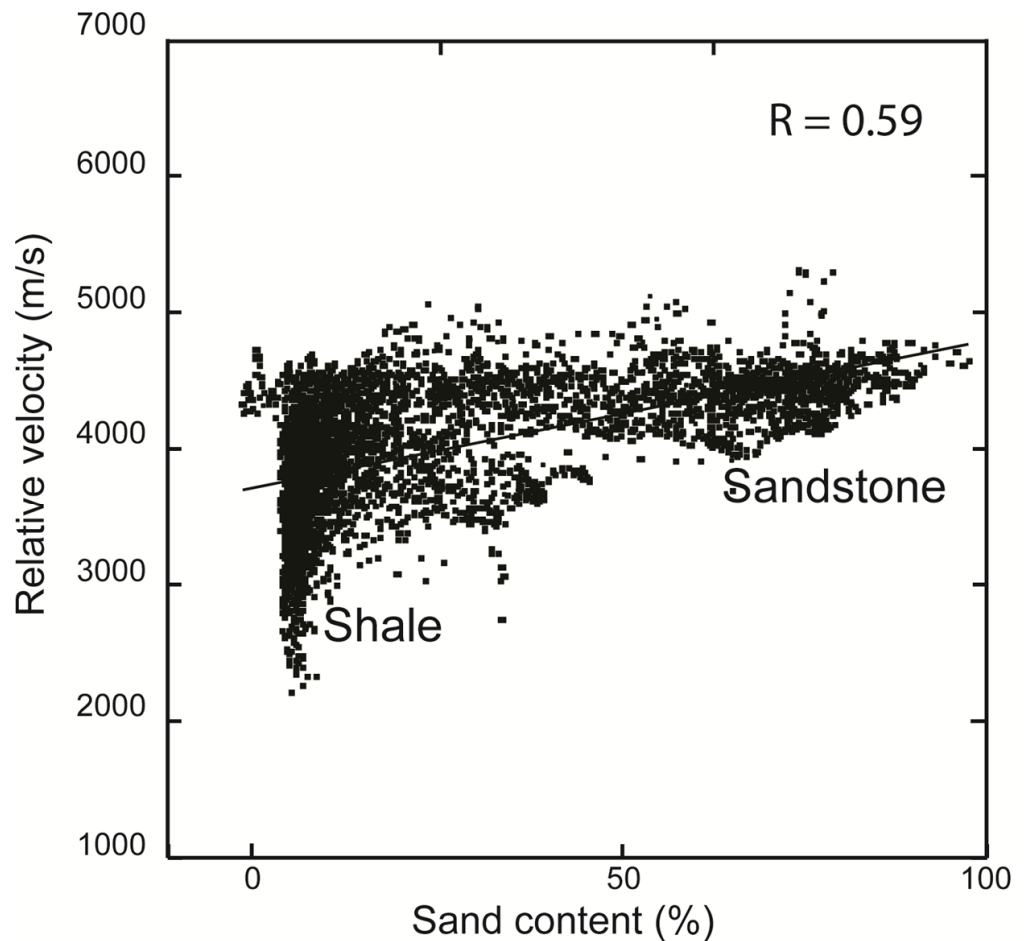
SEISMIC LITHOLOGY

In the study area, the ability to use seismic amplitude as a lithology indicator depends on the acoustic relationships between

sandstone and shale. A petrophysical analysis of the Oscar D. Jochen well indicates that although considerable overlap occurs between sandstones and shale, sandstones are statistically higher in relative (compaction-corrected) velocity (and acoustic imped-ance) relative to shale (Fig. 13). The difference in average value of sandstone velocity and that of shale is moderate (about 500 [m/s]), which generates an average reflection coefficient of 0.05–0.07.

In the study area, most of the Wilcox sandstones are less than 100 ft (30.5 m) thick (Fig. 8). Some off-shelf slope-fan sand bodies are as thick as 165 ft (50 m) (e.g., Oehlke well in Figure 8). Knowing that the dominant frequency of the seismic data is merely about 25 Hz in the study interval, which corresponds to a seismic resolution limit of 131 ft (40 m or 20 ms), most of the sandstone beds are apparently seismically thin. Reflections in a zero-phase volume are proxies for surfaces and are less ideal for thin-bed study. A -90° phasing of seismic traces (Zeng et al., 2007) may enhance the ability to interpret 3D seismic data in terms of lithofacies by converting a seismic amplitude section into a relative acoustic impedance section (Fig. 14A). However, this assertion holds true only if sandstone is detected and interfer-ences from adjacent sand bodies do not surpass the reflection energy of the thin bed itself (e.g., sandstone beds in gray boxes, Fig. 14A). In such a situation, sandstone thickness can also be estimated by constructing an amplitude-thickness relationship if such a relationship can be established for an individual sandstone unit.

Figure 13. Relationship between log-derived relative velocity (after correcting for the compaction effect) and lithology in Oscar D. Jochen well.

QAe4739

For clustered thin-bed packages, which dominate the upper Wilcox (e.g., sandstone beds in yellow box, Fig. 14A), alternative seismic attributes are necessary for lithology identification. It was observed that the root mean square (RMS) amplitude curve (Fig. 14B) is positively correlated to sandstone content (Fig. 15): the stronger the amplitude, the higher the content. By testing various amplitude-derived attributes, it was concluded that instantaneous amplitude (or reflection strength) is an optimal measurement of overall amplitude, and therefore lithology, at high stratigraphic resolution (Figs. 14C and 15). Almost all sandstones, thick or thin, have a relatively higher instantaneous amplitude value compared to shale beds that lie in between them. However, without phase information, thickness is difficult to estimate with instantaneous amplitude. Wells were depended on to provide a general sandstone-thickness range for each mapping unit.

In the following discussions, the instantaneous amplitude is used to analyze lithology and related depositional systems.

STRATAL SLICING

In a formation composed of seismically thin beds, such as in the Wilcox Group, most sandstones, including most of the "thick" IVF sandstone bodies, are merely vertically detected, not resolved, meaning that the sandstones are seen as amplitude events without identification of their tops and bases. Similarly, many higher-order sequence boundaries and maximum-flooding surfaces cannot be accurately correlated manually in 3D. Consequently alternative seismic-sedimentologic approaches were used

for higher-order sequence mapping and facies interpretation. The seismic-attribute (in this study, instantaneous amplitude) patterns on the stratal slices provide critical lithologic and geomorphologic information for high-resolution imaging of depositional systems. The key steps for stratal slicing include selecting geologic time-equivalent seismic-reference events and proportional slicing between the events (Zeng et al., 1998a, 1998b).

The generation of stratal slices in the study area was challenging. Good-quality seismic-chronostratigraphic framework were used to make genuine stratal slices. In the on-shelf portion of the third-order LST where IVFs cut through exposed on-shelf deltaic deposits, and in the third-order TST, faults display little or no growth, and seismic reference events can be correlated throughout the 3D survey without difficulties (e.g., horizons SB1–SB3, Fig. 6). In the deeper section where sediments thicken significantly in subbasins, however, seismic correlation across different subbasins is difficult because of the dischronous nature of the sediments across the subbasins. Ultimately, only seismic reference events in subbasin C were picked where shale ridges and significant LST expansion have been observed (e.g., maximum flooding surface [mfs], Fig. 6).

Two sets of stratal slices were prepared for the on-shelf and off-shelf portions of the seismic data. The on-shelf stratal slices were made among regional reference events SB1–SB3 in most of the 3D survey area; the off-shelf stratal slices were generated among five local reference events (including mfs in Figure 6) in subbasin C. The stratal slices were sampled at an approximated 4 ms (26 ft [8 m]) and therefore provided detailed data relative to the lithology and seismic geomor-
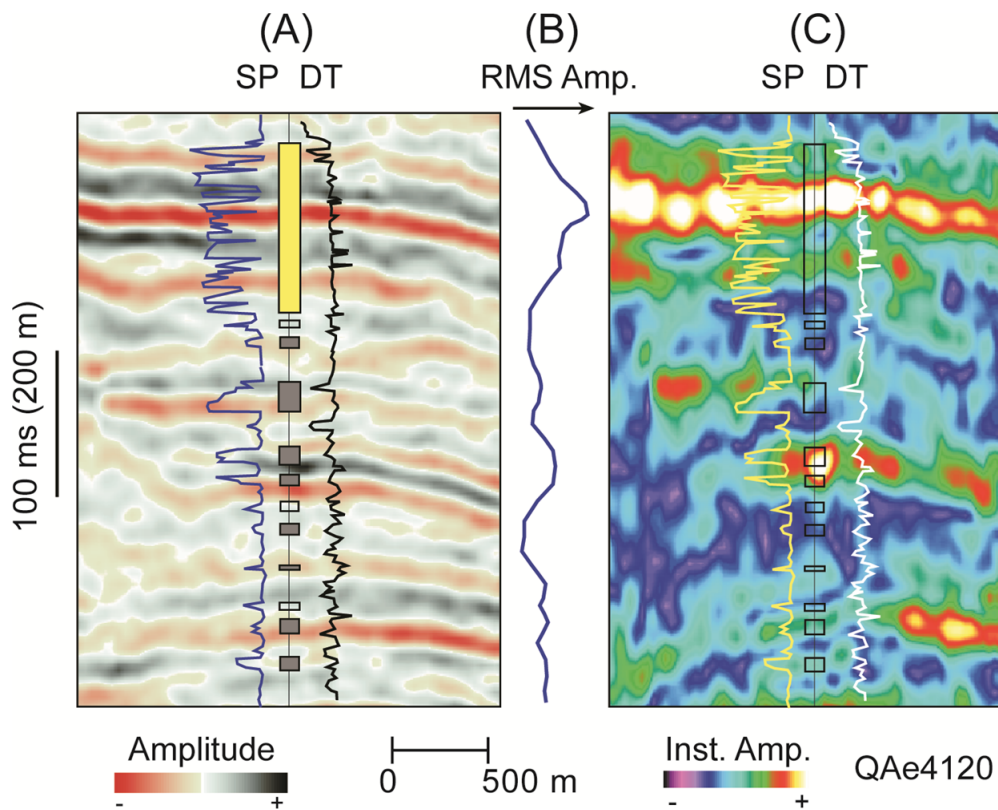
Figure 14. Seismic attributes as an indicator of lithology as seen in well-seismic section. (A) -90° amplitude section tied to spontaneous potential (SP) and compressional slowness (DT) logs in Oscar D. Jochen well. Yellow, grey, and transparent boxes denote clustered, isolated and detected, and undetected sandstone beds, respectively. (B) Root mean square (RMS) amplitude curve calculated from well-site trace in (A). (C) Instantaneous amplitude section calculated from (A). See Figure 3 for well location.
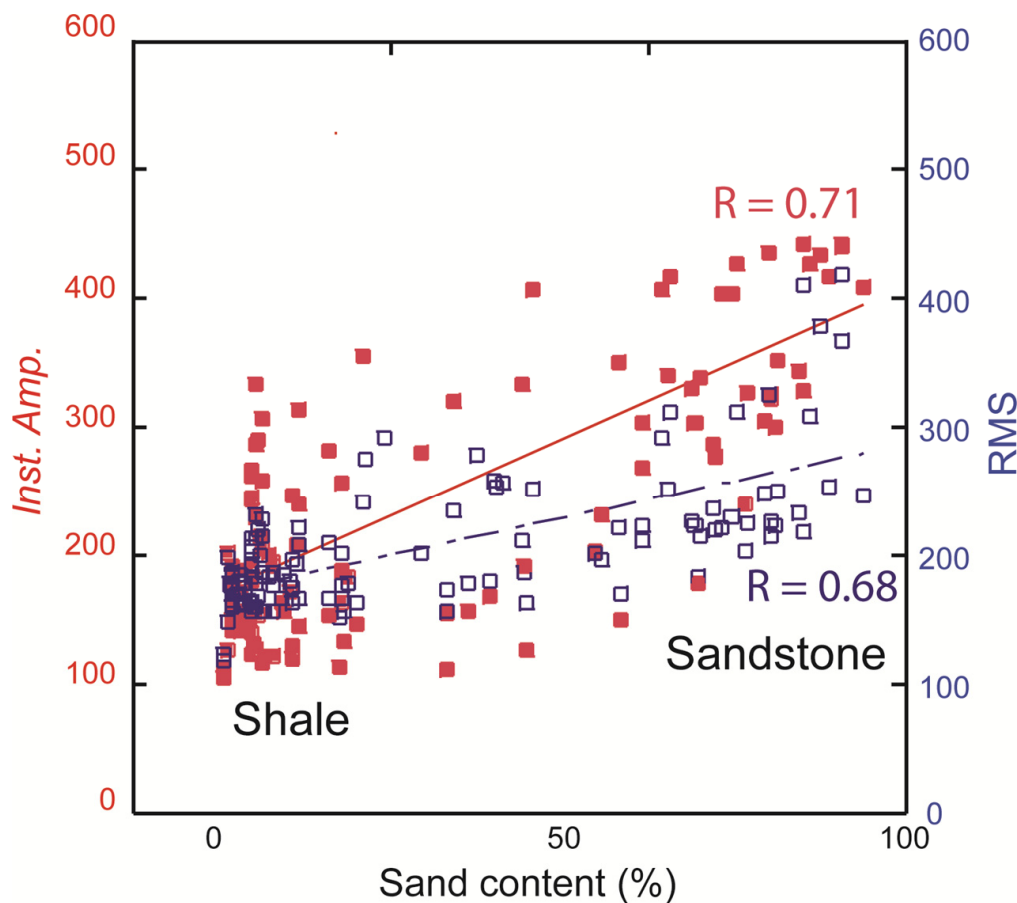
Figure 15. Seismic attributes as an indicator of lithology as seen in cross plots between the sand content calculated from spontaneous potential (SP) curve in Oscar D. Jochen well and well-site root mean square (RMS) amplitude (blue points) and instantaneous amplitude (red points).

phology of depositional elements. For discussion here, four stratal slices were selected for on-shelf IVF/exposed- shelf systems tract (Fig. 16) and another four for the lowstand delta/slope-fan systems tract (Fig. 17). These slices follow a general seismic-event trend but not necessarily any specific seismic peaks or troughs.

SEDIMENT DISPERSAL PATTERNS

Lithology-calibrated seismic geomorphologic patterns on stratal slices are the basis for facies interpretation. Because hori-zontal seismic resolution is roughly the same as vertical seismic resolution (Lindsey, 1989), the horizontal seismic resolution in the seismic data must be at least close to the vertical seismic resolution (one quarter of seismic wavelength, or 131 ft [40 m]). Almost all clastic depositional bodies have a horizontal dimension much larger than vertical dimension (e.g., Galloway and Hobday, 1983). As a result, they are easier to be resolved in horizontal dimension on stratal slices. As will be subsequently demonstrated here, this resolution is enough to resolve horizontal depositional-facies changes within higher-order sequences in the study area.

Figure 16. Stratal slices generated for the on-shelf LST IVF/exposed shelf systems tract. (A) through (D) represents higher-order episodes 1 through 4, respectively. Episodes 1 and 2 are sampled in lower upper Wilcox, and episodes 3 and 4 at Massive and Slick intervals in upper upper Wilcox, respectively (Fig. 2B). Faults are highlighted but amplitude patterns are not interpreted. See Figure 6 for slice position.
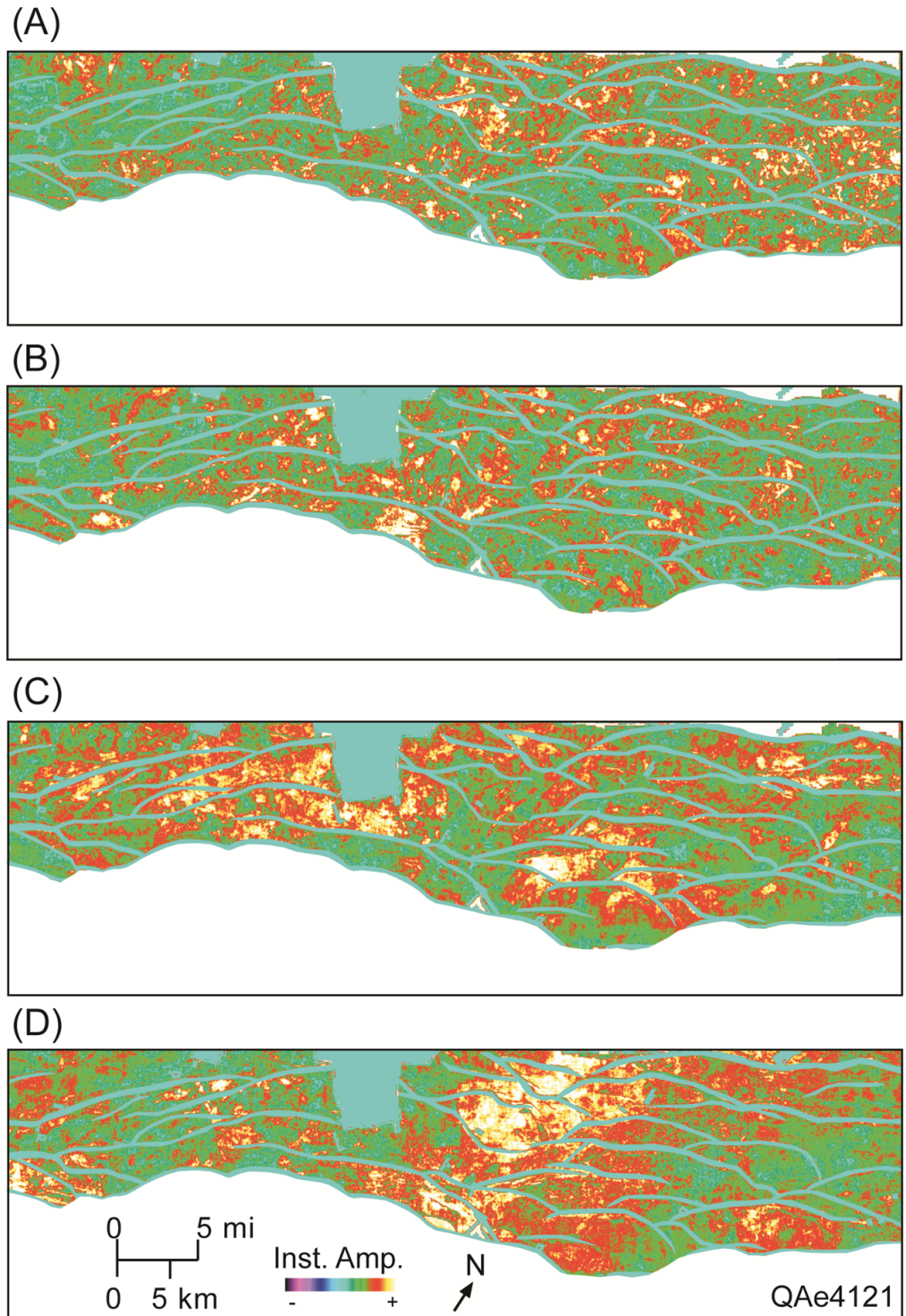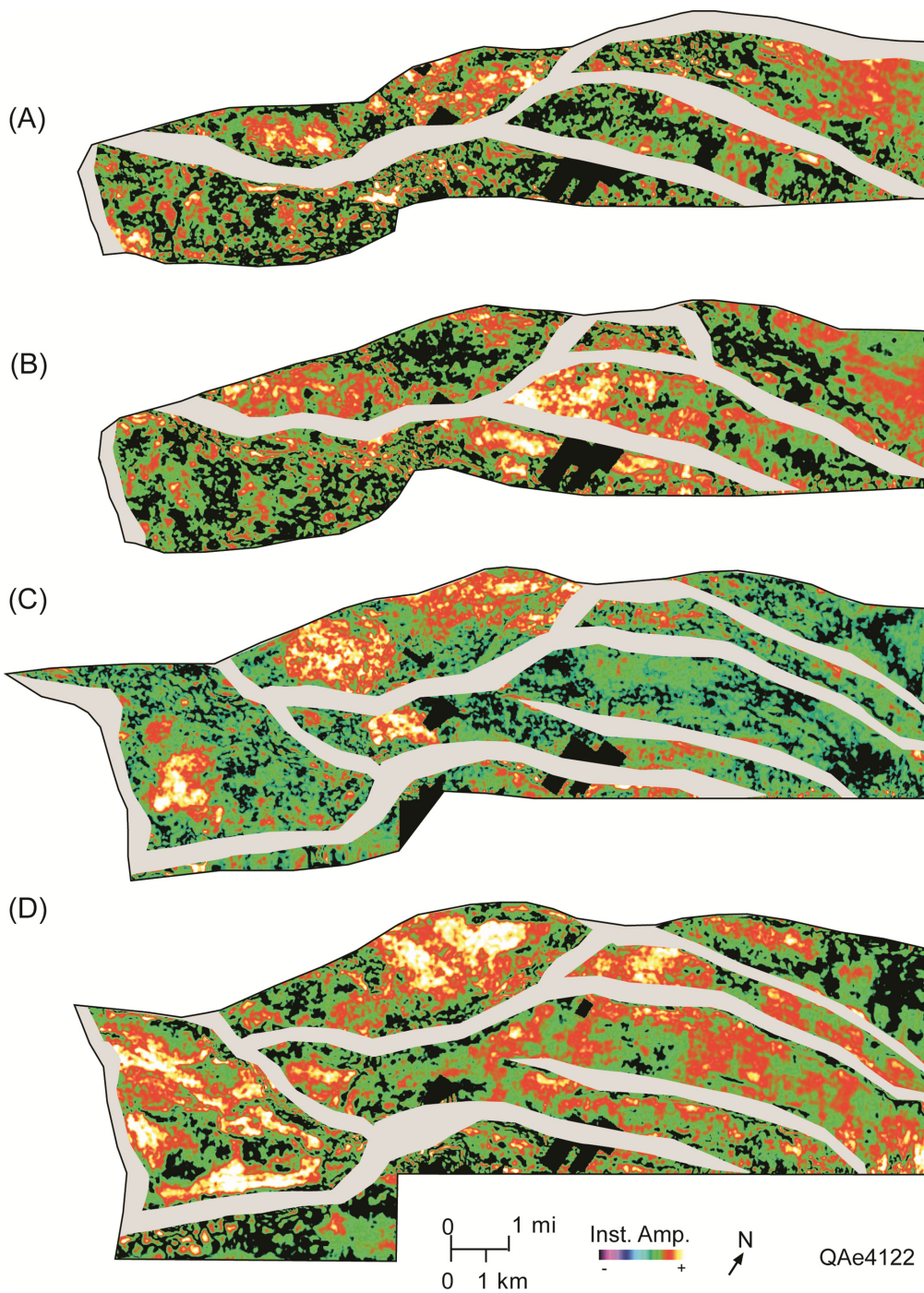
Figure 17. Stratal slices produced for the off-shelf lowstand delta/slope fan systems tract. (A) through (D) represents higher-order units a through d, respectively. Faults are highlighted but amplitude patterns are not interpreted. See Figure 6 for slice position.

Relationship between Seismic Lithology/ Geomorphology and Facies

In this study, core description helped interpretation of a wave-dominated shoreline setting associated with a wave-dominated delta in the Luling interval of the upper Wilcox (Fig. 9). Wireline-log correlation and facies mapping further revealed that lowstand, incised-valley deposits in the upper Luling truncated underlying highstand, lower-coastal-plain, backbarrier, and barrier-core deposits in the lower Luling unit within the upper Wilcox third-order, on-shelf systems tracts (LST IVF and exposed shelf) (Figs. 10 and 11). The sandstone thickness and dispersal patterns discovered from this mapping provided guidance toward recognizing geologically meaningful seismic-geomorphic patterns displayed on the stratal slices (Figs. 16 and 17).

The stratal slice in Figure 18 was selected as most closely tied to the sandy sediments mapped in the Luling interval (Fig. 6) between episode 1 and episode 2 slices (Figs. 6, 16A, and 16B). The strong instantaneous amplitude pattern in the north and northwestern mapping area appears to be part of a dip-elongate geobody that correlates to the thick, blocky IVF sandstones (Clevenger & Quigley No. 1 Knight and Pan American No. 1 McCollum wells, Fig. 11) in the upper Luling interval (Fig. 12). The weaker, defused amplitudes next to the IVFs coincide with shaly, lower-coastal-plain deposits (Hughes No. 1 Oehlke well, Figs. 11 and 12); the strike-oriented bright amplitudes in the south (Fig. 18) highlight the thick, strike-elongate sandstone trend (Hanson Minerals No. 1 Algea Gas Unit well, Fig. 11) deposited in a wave-dominated shoreline environment (Fig. 10).

Figure 18. Instantaneous amplitude stratal slice tied to Luling interval (See Figure 11 for location of the slice in stratigraphic cross section B–B').
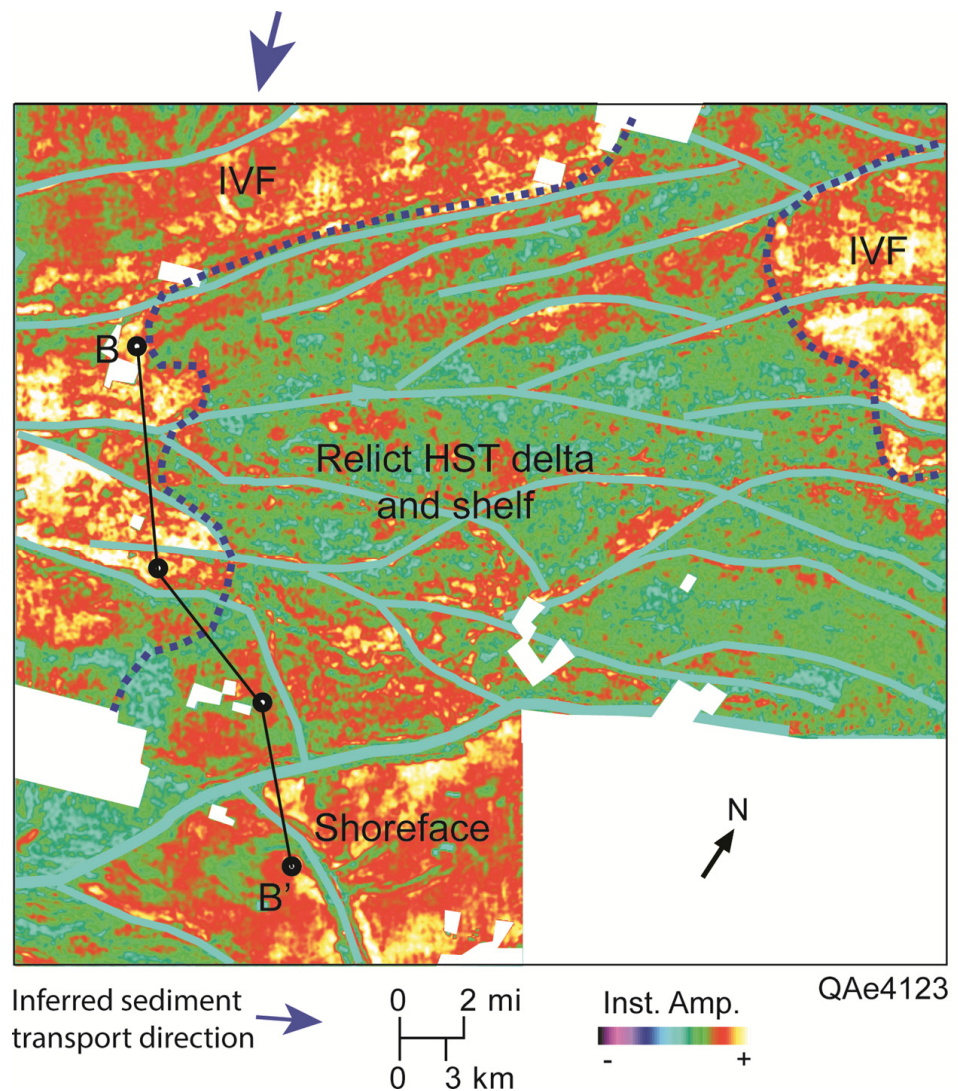
In summary, lithology-calibrated seismic-geomorphologic patterns within the upper Wilcox, third-order, on-shelf systems tracts can be interpreted in terms of depositional facies and environments. In general, high instantaneous amplitudes are inferred to be sandy IVFs (dip-elongate) and wave-dominated deltas and shoreline deposits (strike-elongate), while low amplitudes tend to illustrate shaly, relict highstand delta (lobate-shape) and shelf deposits (shapeless).

The facies interpretation of amplitude patterns within third-order, slope-fan systems tracts was less certain because of the lack of adequate deep wells and core calibration. On the basis of limited well-seismic correlation (e.g., Oehlke well, Fig. 8) and previous studies in Frio subbasins (Hammes et al., 2007; Zeng et al., 2007), it is assumed that the general rules hold true: high-amplitude, lobate, or channel-shaped patterns designate sandy slope fans, while low-amplitude, sheetlike, or random patterns indicate deepwater shale.

On-Shelf Area

The stratal slice series in the on-shelf area disclose no fewer than four higher-order episodes of IVF development on exposed shelf in the upthrown, footwall side of subbasin C (Fig. 19). Despite little sign of seismically resolved channel cutting and erosion in the subparallel seismic package in the vertical seismic section (Fig. 6), these slices display complex yet distinctive in-stantaneous amplitude patterns. As suggested in Figure 18, the bright, higher amplitudes in plan view indicate blocky, sandy sediments (Fig. 11). Interpretation of the high-amplitude patterns in Figure 16 can be tricky, but some common features are recognizable (Fig. 19):

(1) They are predominantly dip-elongate.
(2) They can be straight to highly sinuous.
(3) All of them stop at the boundary fault that separates subbasin C from subbasin B.
(4) Some of them become wider (opened up) along the boundary fault.

As in Figure 19, it is inferred that the bright amplitude patterns in Figure 16 are sand-rich IVFs. In some places, high amplitudes can also indicate sand-rich, highstand deltaic sediments. As a result, the interpreted boundaries of IVFs are somewhat arbitrary and can only be determined accurately with detailed well calibration. Wireline-log mapping (Fig. 12) revealed that the IVFs (e.g., Keller, Bean C Unit, and Luckernbach wells, Fig. 8) are filled with blocky sandstones of fluvial origin. Typically, these sandstones are 33–99 ft (10–30 m) thick in wells, comprising a main framework of sandstones in the units. While most of the IVFs were long (> 15 mi [24.1 km]) and extended beyond the study area to the upstream source areas, some were short with the shape of an estuary. The boundary fault represents the approximate shelf edge at the time of deposition. Toward the shelf edge, the fluvial systems in the IVFs are expected to grade into

Figure 19. Interpreted stratal slices in Figure 16.
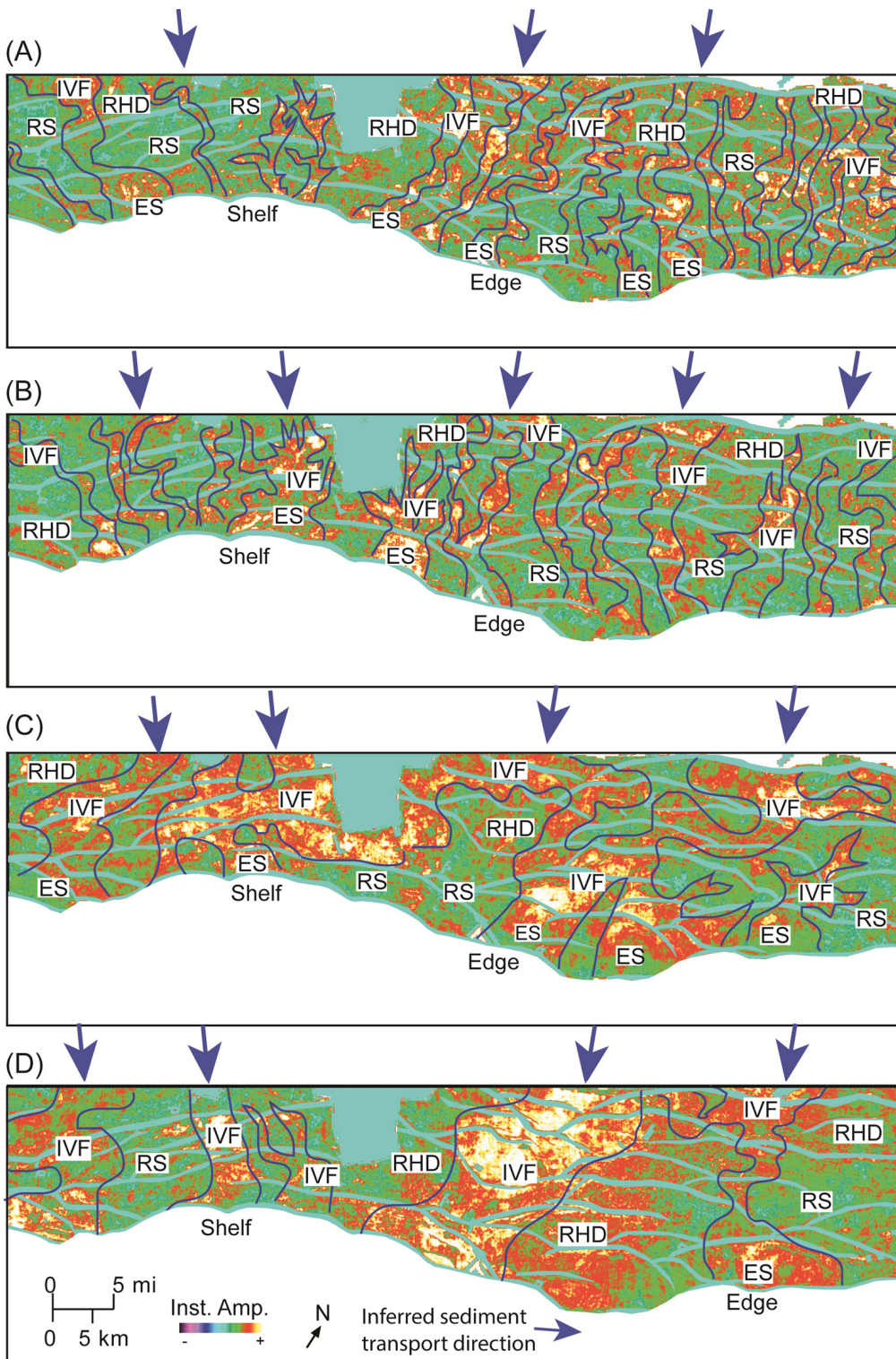
IVF = Incised valley fill
RHD = Relict highstand delta

RS = Relict shelf
ES = Estuary (sandy)

QAe4124

lowstand deltaic or estuary systems. The wells outside the IVFs showed thinner, upward-coarsening, and less sandy sediment in wells (Fig. 11), which implies relict highstand deltaic and shallow-marine sediments preserved on exposed shelf.

Evolution of the IVFs in successive episodes was observed by its changing geometry and size with relative geologic time.

The IVF developed earlier, in episode 1, is 1–2 mi (1.6–3.2 km) in width. The average width increased to 2–3 mi (3.2–4.8 km), 4–6 mi (6.4–9.7 km), and 10 mi (16.1 km) in episodes 2–4, respectively, reflecting a generally upward-coarsening, progradational, continental shelf-building process during upper Wilcox time.

Off-Shelf Area

The stratal slice series in the off-shelf area reveal many higher-order units of lowstand delta (prograding wedge) and slope-fan deposition on the slope of the downthrown, hanging-wall side of subbasin C. Only four units (slices) were interpreted for analyzing sediment-dispersal patterns (Fig. 20).

Excluding largely discontinuous events near the boundary fault and at the domal high, as well as subparallel events in the distal basin (Fig. 6), the lower two slices (Figs. 20A and 20B) contain multiple fanlike, high-amplitude patterns. Fan-size is small (0.5–2 mi [0.8–3.2 km] across). Dip-oriented, sinuous channel patterns are observed in the central and proximal parts of the fans. These fan-shaped amplitudes are mostly correlated to

Figure 20. Interpreted stratal slices in Figure 17.
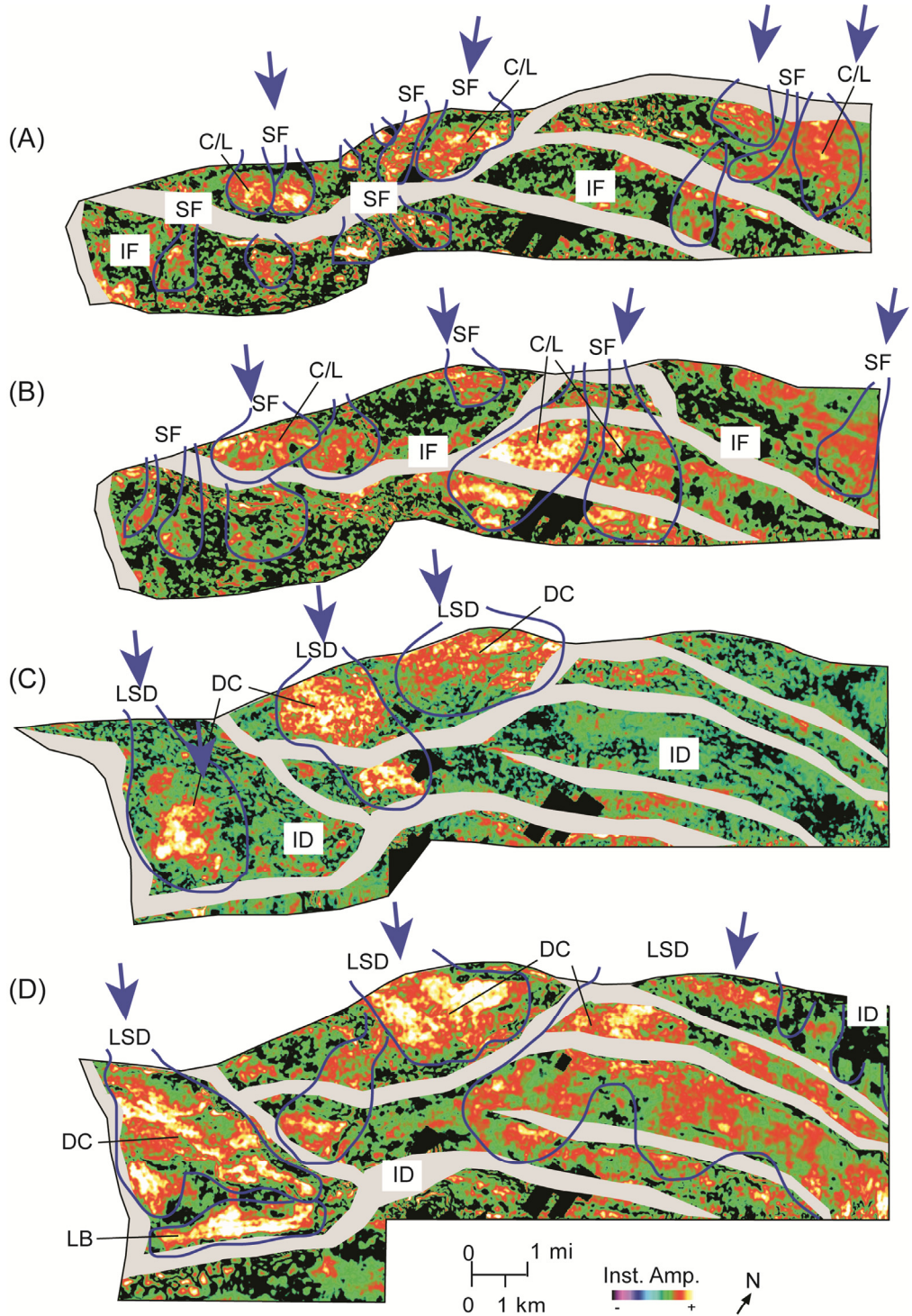
LSD = Lowstand delta
DC = Distributary channel
ID = Interdistributary (mud)
LB = Longshore bar

SF = Slope fan
C/L = Channel/levee
IF = Inter fan

Inferred sediment
transport direction

QAe4125

interbedded sandstones and siltstones in wells (e.g., Oehlke well, Fig. 8). Similar fan-shaped sediment bodies in Frio subbasins are interpreted as deepwater slope-fan turbidite fan systems (Treviño et al., 2003; Brown et al., 2004; Hammes et al., 2004; Zeng et al., 2007). The fan system was inferred to be a lowstand slope-fan system composed of multiple channel/levee elements.

Following a more-continuous seismic-event trend with a clinoformal hint (Fig. 6), the upper two slices (Figs. 20C and 20D) are characterized by lobate amplitude patterns. The size of the high-amplitude lobes is 3–10 mi (4.8–16.1 km) across, greater than that of the slope fans. Straight-to-sinuous channel patterns were observed along their axes. Upward-coarsening and upward-fining motifs in spontaneous potential wireline logs (e.g., May-Holzmark Gas Unit and Oehlke wells, Fig. 8) indicate progradational and channel-fill processes. This system was interpreted as lowstand deltas that were formed when sediments brought by the entrenched river prograded over the upper-slope sediment fill with sea level just below the shelf edge. A strike-oriented amplitude anomaly (Fig. 20D) was inferred to be a longshore bar system related to wave modification. Dip-oriented lobate systems represent fluvial-dominated deltas with uncertain wave reworking.

Link between On-Shelf and Off-Shelf Depositional Systems

Because stratal slices have only relative geologic time meaning, it is a challenge to correlate an LST IVF system in an upthrown, on-shelf area to lowstand delta and slope fans in a downthrown, subbasin area. Lack of detailed biostratigraphic data in wells prevents accurate chronostratigraphic correlation across the boundary fault. A tentative solution is to tie slices on both sides of the boundary fault in a linear and arbitrary time scale (e.g.,

slice pair episode 1/unit a in Figure 21 and episode 4/unit d in Fig. 22).

Stratal slice pair episode 1/unit a (Fig. 21) links approximately equivalent depositional surfaces across the boundary fault during an episode of slope-fan development in subbasin C. As interpreted in Figure 19A, the landward portion of the stratal slice pair displays complex, dip-oriented amplitude patterns, which were interpreted to be IVFs on exposed shelf, filled with sand-rich, mostly sinuous fluvial channel sediments. All channel systems (entrenched rivers) abruptly terminate at the boundary fault, indicating a narrow strike-oriented zone where shelf-edge deltas developed but are poorly preserved. Where an IVF widened in a funnel shape, estuary probably existed. The basinward portion of stratal slice pairs reveals many fanlike amplitude patterns (Fig. 20A), which were interpreted as a lowstand slope-fan system. The observation that multiple dip-oriented fans distributed along the shelf edge implies a point-sourced sediment-dispersal pattern, fed by multiple IVFs on exposed shelf (Fig. 21).

Stratal slice pair episode 4/unit d (Fig. 22) displays seismic-geomorphologic patterns following depositional surfaces across the boundary fault during an episode of lowstand delta deposition in subbasin C. The landward portion of the stratal slice pair (Fig. 19D) demonstrates a dip-oriented channelized system similar to the IVF system in Figure 19A, although with significantly greater size of IVF channels. The seaward portion of the stratal slice pair displays large lobate amplitude patterns (Fig. 20D) with straight-to-sinuous channel patterns along their axes. It is interpreted that this system is composed of lowstand deltas that were formed when sediments brought by the entrenched river prograded over the shelf edge. Similarly, the fact that multiple dip-oriented lowstand delta lobes distributed along the shelf edge implies a point-sourced sediment-dispersal pattern, with sediments provided by multiple IVFs on exposed shelf (Fig. 22).
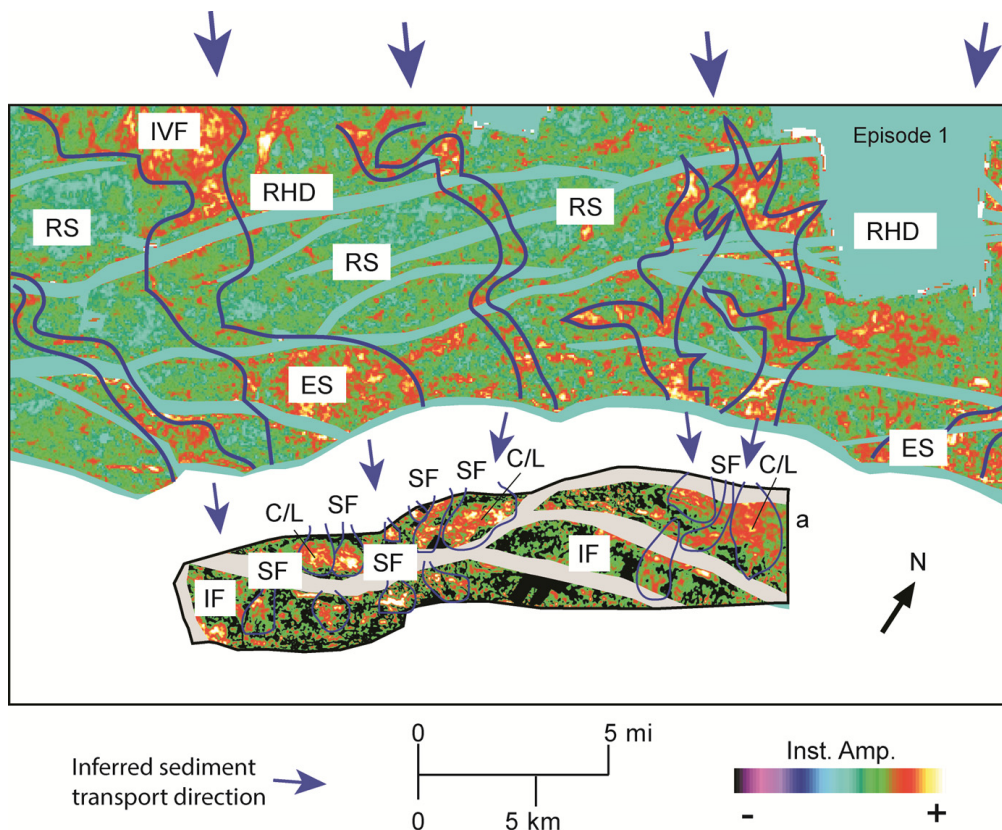

Figure 21. Stratal slice pair (episode 1 in Figure 16 and slice a in Figure 17) showing relationship between on-shelf IVFs and off-shelf lowstand prograding deltas. See Figure 6 for slice pair position.

QAe4127

Figure 22. Stratal slice pair (episode 4 in Figure 16 and slice d in Figure 17) showing relationship between on-shelf IVFs and off-shelf slope fans. See Figure 6 for slice pair position.
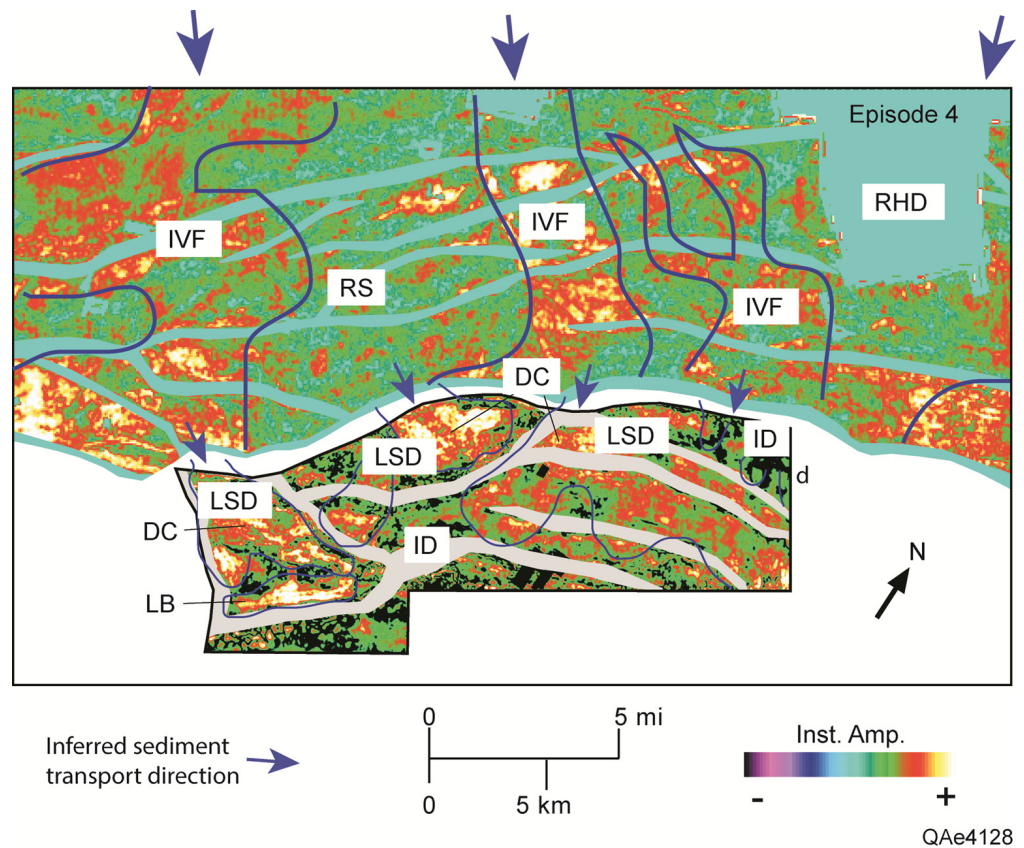
DISCUSSION

The 3D architecture of the Wilcox Group in the south-central Texas coast area can be interpreted within a sequence-stratigraphic framework (Brown and Loucks, 2009). Stratal-stacking patterns defined by Brown et al. (2004, 2005) for the upper Oligocene in Texas and by Mitchum et al. (1993), Hentz and Zeng (2003), and Zeng and Hentz (2004) for the Miocene in Louisiana are similar to what appear in the Wilcox interval. In this study, seismically derived third-order structural and subbasin architecture, wireline log correlation of stratal-stacking patterns, and stratal slices prepared within a time-equivalent, sequence-stratigraphic framework provide critical data for interpreting the depositional systems that display unique sediment-dispersal patterns in individual systems tracts.

Previous studies (Treviño et al., 2003; Brown et al., 2004; Hammes et al., 2004; Zeng et al., 2007) have observed that upper Oligocene Frio subbasins were formed as a result of interaction among sediment supply, shale-triggered growth faulting, and relative sea-level cycles. The Frio Formation is characterized by geologic-time transgression across the third-order lowstand subbasins. Using Frio subbasins as a close analog, it is recognized that third-order lowstand wedges in four subbasins were separated by major growth faults. Filling one subbasin at a time, these third-order lowstand systems tracts are successively younger, from lower Wilcox in the most landward subbasin (subbasin A, Fig. 6) to upper Wilcox in the most seaward subbasins (subbasins C and D, Fig. 6). This interpretation was supported by the indirect correlation between third-order LSTs in seismic sections and sediment-dispersal patterns on stratal slices at opposite sides of the growth faults. However, although log-stacking patterns that define highstand systems tracts (HSTs) and LSTs were consistently applied in well correlations, this correlation scheme was arbitrary because of the lack of biostratigraphic data in wells. Future work is needed to improve the correlation, which is cru-

cial in explaining the sources of sands in the subbasins and of the mobile shale in deeply seated shale ridges.

Compared to previous Wilcox studies (e.g., Fisher and McGowen, 1967; Edwards, 1981; Bebout et al., 1982; Galloway, 2000, 2011), the most significant result of this investigation is the imaging and interpretation of multiple higher-order episodes, lowstand incised valleys filled with sandy fluvial sediments on a large Wilcox exposed shelf. The outline geometry (shape or geobody) of those IVFs and their lateral distribution are clear on seismic stratal slices. However, the limit of seismic resolution prevented the interpretation of internal architecture, e.g., lithofacies groups, cut-and-fill history and local time lines. Madof et al. (2009) reported that gravity-induced slope failure does not necessarily occur only during lowstands. Also, work has been done (Madof et al., 2016) showing that along-strike variability may influence the interpretation of systems tracts. In addition, there has been significant new research on incised valleys in recent decades by means of numerical modeling, physical modeling, outcrop, and subsurface studies (e.g., Blum and Price, 1998; Strong and Paola, 2008; Martin et al., 2009, 2011; Holbrook and Bhattacharya, 2012; Woolf, 2012). Some important observations have been made on incised valley widening/deepening process and forming of multiple channel-belt deposits and composite valley edges. Hopefully, some of those issues can be investigated with high-resolution seismic data in the future.

Recognition of IVFs in the Wilcox Group along the Gulf Coast has significance in predicting LST sandstone reservoirs farther offshore in front of the older Cretaceous shelf margin. Fiduk et al. (1999) reported thick Wilcox basin-floor sandstone reservoirs in the Perdido Fold Belt, an area several hundred miles away from the Wilcox shelf edge. Galloway et al. (2000, 2011) among many others (e.g., Zarra, 2007) identified thick Wilcox basin-floor sandy sediments in the large deepwater Gulf of Mexico frontier area. These sandstones must have been sourced across the exposed Wilcox shelf. The transportation fairways on

exposed shelf, however, might vary in time and by location. Galloway et al. (2000) reported Yoakum Canyon, a large submarine canyon longer than 100 mi (161 km) possibly associated with a submarine fan on the floor of the mouth of the Gulf during upper Wilcox time. Part of the huge sediment influx to the deepwater Gulf of Mexico, however, has to have bypassed some other shallow, sand-rich, incised-valley drainage systems. The results of this study provide some insights into the magnitude (width and thickness), stacking pattern, and sediment-dispersal pattern of such systems, which are quite different from submarine canyons.

The incised valleys identified in upper Wilcox in this large, 960 mi^2 (2500 km^2), study area are seismically thin, commonly filled with sandstones of fluvial origin that are 33–131 ft (10–40 m) thick. These valleys were not directly revealed by seismic terminations (valley cuts), as submarine canyons typically are, but by horizontal patterns (geomorphology) inferred by the geometry and architecture of amplitude anomalies on stratal slices. Multiple episodes of IVF development during a third-order lowstand cycle indicated a higher-order (fourth- and fifth-order) sea-level control on base level and accommodation. Those IVFs terminated at major growth fault along the shelf edge. No large erosional features (gullies or canyons) developed in front of the shelf edge; instead, sandy sediments were dumped along fault-created troughs in footwall blocks, forming slope fans and lowstand deltas. Shelf-margin outbuilding, therefore, was limited by sediment trapping related to extreme vertical expansion across growth faults basinward of the previous Cretaceous margin. Nonetheless, bypassing (spilling) of the sandy sediments into deepwater Gulf of Mexico was still possible when sediment supply outpaced subbasin filling, a process that deserves more studies in the future.

CONCLUSIONS

Like Frio subbasins in the Corpus Christi region, shale tectonics and growth fault controlled subbasins exist in the Wilcox Group of the Bee/Goliad region along the central coastal plain of Texas. In the study area, four third-order lowstand subbasins were recognized by using 3D seismic data with sparse well control. These subbasins are characterized by unique structural style, including shale ridge; growth fault and rollover anticline; and distinctive sequence-stratigraphic architecture, such as on-shelf, thin sheets of LST units and off-shelf, thick wedges of LST delta/slope fan sections across the growth fault.

Higher-order depositional sequences in the subbasins are poorly correlated with seismic events in vertical seismic view. An application of seismic-sedimentologic workflow made it possible to identify depositional elements at higher-order sequence and reservoir level (33–131 ft [10–40 m]). Seismic lithology was realized by calibrating seismic attributes to differentiate sandy lithofacies from shaly facies. An adjustment of seismic wavelet phase to -90° or, more practical in this study, the use of instantaneous amplitude fulfilled the purpose. Interpreting seismic geomorphology on stratal slices can illustrate sedimentary geomorphologic patterns that can be interpreted in terms of depositional elements in high resolution. A combined use of the two techniques can predict not only depositional facies but also lithology and reservoir quality.

In subbasin C, three types of depositional systems were identified at a higher-order sequence. Lowstand slope fans are best recognized by their fanlike depositional morphology and high sand content in sinuous channel forms indicated by instantaneous amplitude and wireline logs in wells. Lowstand prograding deltas are composed of deltaic lobes with sandy lobate forms. Lowstand on-shelf systems are represented by multiple, dip-oriented IVFs filled with sandy fluvial sediments on exposed shelf with previously deposited highstand deltaic systems. Wilcox depositional history in the study area is indicated to have begun with deposits of deepwater slope fans, followed by the development of shallow-water lowstand deltas and then of IVFs and relict on-shelf deltas on exposed shelf.

Identification of IVFs in the Wilcox Group along the Gulf Coast can help predict LST sandstone reservoirs farther offshore in front of the older Cretaceous shelf margin. In the study area, the incised valleys in upper Wilcox are seismically thin and were not revealed by erosional features on seismic sections. Multiple episodes of IVF development during a third-order lowstand cycle indicate a higher-order sea-level control on base level and accommodation. Unlike large, deep submarine canyons (e.g., Yoakum Canyon), those IVFs may have provided alternative pathways for a large amount of sandy sediments being transported into deepwater Gulf of Mexico during Wilcox time.

ACKNOWLEDGMENTS

REFERENCES CITED

Aconcha, E. S., C. Kerans, and H. Zeng, 2008, Seismic geomorphology applied to Lower Glen Rose patch reefs in the Maverick Basin, southwest Texas: Gulf Coast Association of Geological Societies Transactions, v. 58, p. 3–23.

Ambrose, W. A., T. F. Hentz, F. Bonnaffé, R. G. Loucks, L. F. Brown, Jr., F. P. Wang, and E. C. Potter, 2009, Sequence stratigraphic controls on complex reservoir architecture of highstand fluvial-dominated deltaic and lowstand valley-fill deposits in the Woodbine Group, East Texas Field: Regional and local perspectives: American Association of Petroleum Geologists Bulletin, v. 93, p. 231–269.

Bebout, D. G., B. R. Weise, A. R. Gregory, and M. B. Edwards, 1982, Wilcox sandstone reservoirs in the deep subsurface along the Texas Gulf Coast: Their potential for production of geopressured geothermal energy: Texas Bureau of Economic Geology Report of Investigations 117, Austin, 125 p.

Blum, M. D., and D. M. Price, 1998, Quaternary alluvial plain construction in response to glacio-eustatic and climatic controls, Texas Gulf Coastal Plain, in K. W. Shanley and P. J. McCabe, eds., Relative role of eustasy, climate and tectonism in continental rocks: Society of Economic Paleontologists and Mineralogists Special Publication 59, Tulsa, Oklahoma, p. 31–48.

Boothroyd, J. C., 1972, Coarse-grained sedimentation on a braided outwash fan, northeast Gulf of Alaska: University of South Carolina Coastal Research Division Technical Report 6, Columbia, 127 p.

Brown Jr., L. F., and R. G. Loucks, 2009, Chronostratigraphy of Cenozoic depositional sequences and systems tracts: A Wheeler chart of the northwest margin of the Gulf of Mexico Basin: Texas Bureau of Economic Geology Report of Investigations 273, Austin, 28 p.

Brown, L. F., Jr., R. G. Loucks, R. H. Treviño, and U. Hammes, 2004, Understanding growth-faulted, intraslope subbasins by applying sequence-stratigraphic principles: Examples from the south Texas Oligocene Frio Formation: American Association of Petroleum Geologists Bulletin, v. 88, p. 1501–1522.

Brown, L. F., Jr., R. G. Loucks, and R. H. Treviño, 2005, Site-specific sequence-stratigraphic section benchmark charts are key to regional chronostratigraphic systems tract analysis in growth-faulted basins: American Association of Petroleum Geologists Bulletin, v. 89, p. 715–724.

Carter, D. C., 2003, 3-D seismic geomorphology: Insights into fluvial reservoir deposition and performance, Widuri Field, Java Sea: American Association of Petroleum Geologists Bulletin, v. 87, p. 909–934.

Cheng, S., Y. Jiang, J. Li, C. Li, Y. Wang, and L. Xu, 2015, Reservoir prediction in a development area with a high-density well pattern using seismic sedimentology: An example from the BB2 Block, Changyuan LMD Oil Field, Songliao Basin, China: Interpretation, v. 3, no. 3, p. SS87–SS99.

Edwards, M. B., 1981, The Live Oak delta complex: An unstable, shelf/edge delta in the deep Wilcox trend of South Texas: American Association of Petroleum Geologists Bulletin, v. 65, p. 54–73.

Fiduk, J. C., and 10 co-authors, 1999, The Perdido Fold Belt, northwestern deep Gulf of Mexico: Part 2. Seismic stratigraphy and petroleum systems: American Association of Petroleum Geologists Bulletin, v. 83, p. 578–612.

Fisher, W. L., and J. H. McGowen, 1967, Depositional systems in the Wilcox Group of Texas and their relationship to occurrence of oil and gas: Gulf Coast Association of Geological Societies Transactions, v. 17, p. 105–125.

Fulthorpe, C. S., W. E. Galloway, J. W. Snedden, P. E. Ganey-Curry, and T. L. Whiteaker, 2014, New insights into Cenozoic depositional systems of the Gulf of Mexico Basin: Gulf Coast Association of Geological Societies Transactions, v. 64, p. 119–129.

Galloway, W. E., 1977, Catahoula Formation of the Texas Coastal Plain—Depositional systems, composition, structural development, ground-water flow history, and uranium distribution: Texas Bureau of Economic Geology Report of Investigations 87, Austin, 59 p.

Galloway, W. E., P. E. Ganey-Curry, X. Li, and R. T. Buffler, 2000, Cenozoic depositional history of the Gulf of Mexico Basin: American Association of Petroleum Geologists Bulletin, v. 84, no. 11, p. 1743–1774.

Galloway, W. E., T. L. Whiteaker, and P. E. Ganey-Curry, 2011, History of Cenozoic North American drainage basin evolution, sediment yield, and accumulation in the Gulf of Mexico Basin: Geosphere, v. 7, p. 938–973.

Galloway, W. E., and D. K. Hobday, 1983, Terrigenous clastic depositional systems: Applications to petroleum, coal, and uranium exploration: Springer-Verlag, New York, New York, 423 p.

Hammes, U., R. G. Loucks, L. F. Brown, R. H. Treviño, R. L. Remington, and P. Montoya, P., 2004, Structural setting and sequence architecture of a growth-faulted lowstand subbasin, Frio Formation, South Texas: Gulf Coast Association of Geological Societies Transactions, v. 54, p. 237–246.

Hammes, U., H. Zeng, R. G. Loucks, and L. F. Brown, Jr., 2007, All fill—No spill: Slope-fan sand bodies in growth-faulted subbasins: Oligocene Frio Formation, South Texas Gulf Coast: Gulf Coast Association of Geological Societies Transactions, v. 57, p. 361–371.

Hargis, R. N., 2009, Major transgressive shales of the Wilcox, northern portion of South Texas: South Texas Geological Society Bulletin, April 2009 issue, San Antonio, p. 19–47.

Hentz, T. F., and H. Zeng, 2003, High-frequency Miocene sequence stratigraphy, offshore Louisiana: Cycle framework and influence on production distribution in a mature shelf province: American Association of Petroleum Geologists Bulletin, v. 87, p. 197–230.

Holbrook, J. M., and J. P. Bhattacharya, 2012, Reappraisal of the sequence boundary in time and space: Case and considerations for an SU (subaerial unconformity) that is not a sediment bypass surface, a time barrier, or an unconformity: Earth-Science Reviews, v. 113, p. 271–302.

Lindsey, J. P., 1989, The Fresnel zone and its interpretive significance: The Leading Edge, v. 8, no. 10, p. 33–39.

Loucks, R. G., B. T. Moore, and H. Zeng, 2011, On-shelf lower Miocene Oakville sediment-dispersal patterns within a three-dimensional sequence-stratigraphic architectural framework and implications for deep-water reservoirs in the central coastal area of Texas: American Association of Petroleum Geologists Bulletin, v. 95, p. 1795–1817.

Lunt, I. A., J. S. Bridge, and R. S. Tye, 2004, A quantitative, three-dimensional depositional model of gravelly braided rivers: Sedimentology, v. 51, p. 377–414.

Martin, J., A. Cantelli, C. Paola, M. Blum, and M. Wolinsky, 2011, Quantitative modeling of the evolution and geometry of incised valleys: Journal of Sedimentary Research, v. 81, p. 64–79.

Martin, J., C. Paola, V. Abreu, J. Neal, and B. Sheets, 2009, Sequence stratigraphy of experimental strata under known conditions of differential subsidence and variable base level: American Association of Petroleum Geologists Bulletin, v. 93, p. 503–533.

Mitchum, R. M., Jr., J. B. Sangree, P. R. Vail, and W. W. Wornardt, 1993, Recognizing sequences and systems tract from well logs, seismic data, and biostratigraphy: Examples from the late Cenozoic of the Gulf of Mexico, in P. Weimer and H. Posamentier, eds., Siliciclastic sequence stratigraphy: Recent developments and applications: American Association of Petroleum Geologists Memoir 58, Tulsa, Oklahoma, p. 163–197.

Madof, A. S., N. Christie-Blick, and M. H. Anders, 2009, Stratigraphic controls on a salt-withdrawal intraslope minibasin, north-central Green Canyon, Gulf of Mexico: Implications for misinterpreting sea level change: American Association of Petroleum Geologists Bulletin, v. 93, p. 535–561.

Madof, A. S., A. D. Harris, and S. D. Connell, 2016, Nearshore along-strike variability: Is the concept of the systems tract unhinged?: Geology, v. 44, p. 315–318.

Montgomery, S. L., 1997, Bob West Field: Extending upper Wilcox production in South Texas: American Association of Petroleum Geologists Bulletin, v. 81, p. 697–710.

Ore, H. T., 1963, Some criteria for recognition of braided stream deposits: Wyoming University Department of Geology Contributions to Geology 3, Laramie, p. 1–14.

Posamentier, H. W., 2000, Seismic stratigraphy into the next millennium; a focus on 3D seismic data: American Association of Petroleum Geologists Search and Discovery Article 90914, Tulsa, Oklahoma, <http://www.searchanddiscovery.com/abstracts/html/2000/annual/abstracts/0537.htm> Last Accessed August 18.

Posamentier, H. W., 2001, Seismic geomorphology and depositional systems of deep water environments; observations from offshore Nigeria, Gulf of Mexico, and Indonesia: American Association of Petroleum Geologists Search and Discovery Article 90906, Tulsa, Oklahoma, <http://www.searchanddiscovery.com/abstracts/html/2001/annual/abstracts/0635.htm> Last Accessed August 18.

Schumm, S. A., 1981, Evolution and response of the fluvial system, sedimentological implications, in F. G. Ethridge and R. M. Flores, eds., Recent and ancient non-marine depositional environments: models for exploration: Society of Economic Paleontologists and Mineralogists Special Publication 31, Tulsa, Oklahoma, p. 19–29.

Smith, N. D., 1970, The braided stream depositional environment: comparison of the Platte River with some Silurian clastic rocks, north-central Appalachians: Geological Society of America Bulletin, v. 81, p. 2993–3014.

Strong, N., and C. Paola, 2008, Valleys that never were: Time surfaces versus stratigraphic surfaces: Journal of Sedimentary Research, v. 78, p. 579–593.

Treviño, R. H., R. G. Loucks, L. F. Brown, Jr., and R. L. Remington, 2003, General geology of the mid-Tertiary Block 889 Field area, offshore Mustang Island, Texas: Gulf Coast Association of Geological Societies Transactions, v. 53, p. 802–814.

Van Wagoner, J. C., R. M. Mitchum, K. M. Campion, and V. D. Rahmanian, 1990, Siliciclastic sequence stratigraphy in well logs, cores, and outcrops: Concepts for high-resolution correlation of time and facies: American Association of Petroleum Geologists Methods in Exploration Series 7, Tulsa, Oklahoma, 55 p.

Woolf, K. S., 2012, Regional character of the lower Tuscaloosa Formation depositional systems and trends in reservoir quality: Ph.D. Dissertation, University of Texas at Austin, 226 p.

Zarra, L., 2007, Chronostratigraphic framework for the Wilcox Formation (Upper Paleocene–Lower Eocene) in the deep-water

Gulf of Mexico: Biostratigraphy, sequences, and depositional systems, *in* L. Kennen, J. Pindell, and N. C. Rosen, eds., The Paleogene of the Gulf of Mexico and Caribbean basins: Processes, events, and petroleum systems: Proceedings of the 27th Annual Gulf Coast Section of the Society of Economic Paleontologists and Mineralogists Foundation Bob F. Perkins Research Conference Proceedings, Houston, Texas, p. 81–145.

Zeng, H., M. M. Backus, K. T. Barrow, and N. Tyler, 1998a, Stratal slicing: Part I. Realistic 3-D seismic model: Geophysics, v. 63, p. 502–513.

Zeng, H., S. C. Henry, and J. P. Riola, 1998b, Stratal slicing: Part II. Real seismic data: Geophysics, v. 63, p. 514–522.

Zeng, H., and T. F. Hentz, 2004, High-frequency sequence stratigraphy from seismic sedimentology: Applied to Miocene, Vermilion Block 50, Tiger Shoal area, offshore Louisiana: American Association of Petroleum Geologists Bulletin, v. 88, p. 153–174.

Zeng, H., R. G. Loucks, and L. F. Brown, Jr., 2007, Mapping sediment-dispersal patterns and associated systems tracts in fourth- and fifth-order sequences using seismic sedimentology: Example from Corpus Christi Bay, Texas: American Association of Petroleum Geologists Bulletin, v. 91, p. 981–1003.

Zeng, H., W. A. Ambrose, Z. Yin, and W. Xu, 2014, Shale tectonics controlled depositional history, Eocene Wilcox Group, central South Texas coast: Gulf Coast Association of Geological Societies Transactions, v. 64, p. 463–471.